Mechanistic insight of white carbon black in regulating hydration and improving water resistance of magnesium oxysulfate (MOS) cement

Kairong Jin, Hailong Wang, Huijun Xue, Dezhi Wang, Wanli Bi, Wei Wang, Xiangming Zhou

PII: S2352-7102(26)01780-8

DOI: https://doi.org/10.1016/j.jobe.2026.116958

Reference: JOBE 116958

To appear in: *Journal of Building Engineering*

Received Date: 3 May 2026

Revised Date: 2 July 2026

Accepted Date: 20 July 2026

Please cite this article as: K. Jin, H. Wang, H. Xue, D. Wang, W. Bi, W. Wang, X. Zhou, Mechanistic insight of white carbon black in regulating hydration and improving water resistance of magnesium oxysulfate (MOS) cement, *Journal of Building Engineering*, https://doi.org/10.1016/j.jobe.2026.116958.

Mechanistic insight of white carbon black in regulating hydration and improving water resistance of magnesium oxysulfate (MOS) cement

Kairong Jin[1,2,3,4]*, Hailong Wang[1,2,3,4], Huijun Xue[1,2,3,4], Dezhi Wang[5], Wanli Bi[6], Wei Wang[7], Xiangming Zhou[8]*

(1 State Key Laboratory of Water Engineering Ecology and Environment in Arid Area, Inner Mongolia Agricultural University, Hohhot, Inner Mongolia, 010018, PR China; 2 College of Water Conservancy and Civil Engineering, Inner Mongolia Agricultural University, Hohhot, Inner Mongolia, 010018, PR China; 3 Autonomous Region Collaborative Innovation Center for Integrated Management of Water Resources and Water Environment in the Inner Mongolia Reaches of the Yellow River, Hohhot, Inner Mongolia, 010018, PR China; 4 Inner Mongolia Key Laboratory of Ecohydrology and High-Efficient Utilization of Water Resources, College of Water Conservancy and Civil Engineering, Inner Mongolia Agricultural University, Hohhot, Inner Mongolia, 010018, PR China; 5 School of Civil and Hydraulic Engineering, Ningxia University, Yinchuan, Ningxia, 750021, PR China; 6 College of Materials and Metallurgy, University of Science and Technology Liaoning, Anshan, Liaoning, 114051, PR China; 7 Ningxia Construction Project Quality and Safety General Station, Yinchuan, Ningxia, 750021, PR China; 8 Department of Civil & Environmental Engineering, Brunel University of London, Uxbridge, Middlesex UB8 3PH, United Kingdom)

*Corresponding author: Kairong Jin, Xiangming Zhou

E-mail: yefeng981904494@163.com, xiangming.zhou@brunel.ac.uk

Abstract: As a relatively new type of eco-friendly material, magnesium oxysulfate (MOS) cement offers a sustainable alternative to Portland cement. However, its poor water resistance poses a significant challenge to its wider applications. White carbon black (FS) predominantly consists of SiO_2 and exhibits a low degree of crystallinity. This study investigated the mechanism by which FS enhances the strengths and water resistance of MOS cement, using a range of characterisation techniques (NMR, HR-TEM, XPS, etc.). FS actively participated in the hydration of MOS cement by consuming the OH^- released by MgO hydration or $Mg(OH)_2$, therefore transforming them into magnesium silicate hydrate gel, while also influencing the content of the $5Mg(OH)_2 \cdot MgSO_4 \cdot 7H_2O$

phase, which exhibited adsorption of magnesium silicate hydrate gel on its surface, resulting in an intertwinement at the nanoscale between it and the magnesium silicate hydrate gel and increased in both compressive and flexural strength, as well as demonstrating compatibility. Additionally, the magnesium silicate hydrate gel provided partial protection against the decomposition of $5Mg(OH)_2 \cdot MgSO_4 \cdot 7H_2O$ phase upon water immersion. As the proportion of $MgO/Mg(OH)_2$ participating in the reaction varied, the resulting magnesium silicate hydrate exhibited corresponding shifts in its Mg/Si composition. The ongoing production of magnesium silicate hydrate gel under water immersion led to a 75.76% increase in the compressive strength of MOS cement, with the resulting gel's structure progressively approaching that of talc (T:O:T). A mechanism model of synergetic hydration of MOS cement with FS is proposed to elaborate on the findings.

Keywords: Magnesium oxysulfate cement; White carbon black; Phase composition; Water resistance; Magnesium silicate hydrate gel

1 Introduction

As global warming accelerates, reducing carbon dioxide emissions from industrial activities has become a crucial strategy for mitigating or altering the increasing global warming trend, particularly due to the significant negative impacts of temperature rise on crop production and human livelihoods [1]. Cement and concrete play a pivotal role in infrastructure development, with their production contributing approximately 8% of global CO_2 emissions resulting from human activities [2]. Producing Portland cement involves calcining limestone at temperatures close to 1450 °C to obtain clinker, an energy-hungry process that is also responsible for large-scale CO_2 release [3]. However, the raw materials used to produce magnesium oxide-based cement need a much lower calcination temperature, indicating a lower carbon footprint under certain conditions.

Magnesium oxysulfate (MOS) cement represents a new class of eco-friendly binders, conventionally made from lightly calcined MgO, epsom salt, and water-a formulation consistent with the low-carbon cement strategy [4]. However, the phases within MOS cement, including the $3Mg(OH)_2 \cdot MgSO_4 \cdot 8H_2O$ phase, the $Mg(OH)_2 \cdot MgSO_4 \cdot 5H_2O$ phase, and others, which contribute to its strength gain, exhibit instability at room temperature, thereby restricting its potential

engineering applications [5]. Introducing specific chemical additives into the MOS cement mix is recognized as an efficient method to enhance both compressive strength and resistance to water degradation [6]. When citric acid (CA) is incorporated into MOS cement hydration, it promotes the formation of an additional 5·1·7 phase, contributing to significant mechanical strengthening [7]. In the case of tartaric acid, the extension of setting time encourages the growth of the 5·1·7 phase while hindering $Mg(OH)_2$ precipitation, which collectively improves the final compressive strength [8]. With a 1% addition, boric acid delayed the onset of setting in MOS cement to 73 min, relative to the shorter period recorded for the unmodified counterpart. The retarded initial setting stems from boric acid's ability to suppress the hydration temperature, slowing the overall reaction and allowing more time for the crystalline 5·1·7 phase to grow [9]. Sodium malate binds magnesium ions, thereby inhibiting the formation of $Mg(OH)_2$ and encouraging the growth of the 5·1·7 crystalline phase, which ultimately leads to enhanced flexural strength and water resistance in the resulting cementitious matrix [10]. Similar to weak acids, their salts also govern the hydration process of MOS cement by fostering the generation of the 5·1·7 crystalline phase, which in turn enhances the resulting composite's mechanical performance and water stability [11,12]. That said, when manufacturing magnesium oxysulfate cement, an overly high proportion of LBM is sometimes used, resulting in unstable moisture resistance in particular environments [10,11]. Incorporating mineral admixtures into MOS cement proves to be an effective approach for improving the situation.

Flue gas desulfurization gypsum serves as a substitute for magnesium sulfate in manufacturing MOS cement. It has been observed that flue gas desulfurization gypsum provides the spatial framework necessary for 5·1·7 phase nucleation, an effect that promotes M-S-C-H gel generation while simultaneously moderating the hydration temperature of cement. This is instrumental in elevating the engineering properties and water stability of the resulting MOS cement composite [13]. The addition of phosphogypsum to MOS cement effectively suppresses $Mg(OH)_2$ growth while promoting 5·1·7 phase development, ultimately improving the binder's water resistance [14]. Hydromagnesite reacts with the residual MgO within the MOS cement matrix, promoting the formation of magnesium carbonate. This reaction contributes to the increase in the strength of the MOS cement and enhances its stability upon immersion in water [15]. Steel slag is reused through carbonation in the production of MOS cement, leading to the formation of

an amorphous Ca-Mg-C phase. This phase refines the pore structure of MOS cement, yielding a denser matrix and markedly improved water resistance [16]. The carbonation behavior of magnesium slag, when integrated into MOS cement composites, generates reaction products that promote magnesium silicate hydrate gel formation. This, in turn, exhausts the $Mg(OH)_2$ and MgO present in the matrix, resulting in superior water resistance performance [17]. Ground granulated blast furnace slag contributes to enhanced water resistance in MOS cement through accelerated MgO depletion and magnesium silicate hydrate gel formation, thus making it possible to fabricate a cement with improved long-term durability [18]. Driving the depletion of $Mg(OH)_2$ or remaining MgO within the matrix enhances both the mechanical strength and waterproofing performance of MOS cement. Mineral admixtures, through their hydration activity, can promote the transformation of these leftover phases into a gelling product, offering an effective pathway for further enhancement.

Promoting M-S-H gel formation in MOS cement matrices using magnesium slag or silicic acid has been documented as an effective means of property enhancement, yet both materials are hampered by either unstable sourcing (being industrial by-products) or high cost [17,19]. Considering this, it is essential to explore stable or low-cost materials for enhancing the performance of MOS cement to facilitate its practical application in engineering fields. White carbon black (FS), an industrial material with a high specific surface area, shows potential hydration reactivity in a highly alkaline environment and, more importantly, features low cost, a reliable source and stable properties. This reactive behaviour creates an avenue for exhausting leftover MgO within the binder matrix. In this study, FS was incorporated into the MOS cement manufacturing process. An investigation into the hydration products, strength, and pore size distribution of cement was conducted to elucidate the mechanisms driving gains in strength and water resistance, thus providing a promising route for elevating its engineering performance.

2 Materials and methods

2.1 Materials

FS and LBM used for this study were acquired from Wanhua Tianhe Co., Ltd. in Shandong and Liaoning provinces, respectively. The chemical compositions of FS and LBM are given in Table 1; LBM comprises 63.2% by mass active MgO (a-MgO) based on the hydration method [7].

The data indicate that FS consists mainly of Si-bearing minerals. Citric acid (an analytical reagent (AR)) and $MgSO_4 \cdot 7H_2O$ were sourced from Xilong Co., Ltd.

Table 1 Chemical compositions (*wt%*) of LBM and FS

Components	MgO	Al_2O_3	SiO_2	K_2O	CaO	Fe_2O_3	Na_2O	Others
LBM	93.2	0.33	3.76	0.01	1.74	0.53	-	0.43
FS	0.02	0.58	97.40	0.02	0.07	0.06	0.87	0.98

Fig. 1 presents the XRD pattern and FTIR spectra of FS, while Fig. 2 shows its SEM image. Table 1 details the chemical composition of FS, which contains a substantial amount of SiO_2, i.e. reaching 97.40% by mass. Based on the data from Fig. 1(a) and Fig. 2, it can be concluded that a portion of the SiO_2 exists in an amorphous form. In Fig. 1(b), the signals at 806 cm^{-1} and 1104 cm^{-1} correspond to the symmetric and anti-symmetric stretching modes of Si–O–Si bonds, respectively. Meanwhile, the bands at 3421 cm^{-1} and 1631 cm^{-1} arise from the O–H stretching vibration and the H–O–H bending mode, in that order [19]. The signal observed at 970 cm^{-1} is ascribed to the stretching vibration absorption of Si-OH groups, providing evidence that a portion of the SiO_2 present was not in its crystalline form, which corresponds to the phenomenon observed in Fig. 1(a).

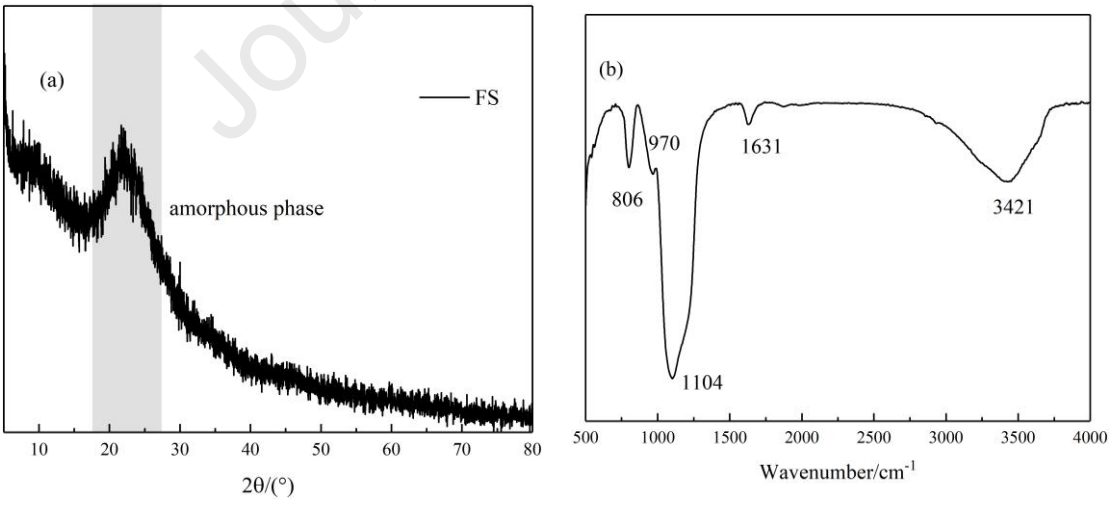

Fig. 1 XRD pattern and FTIR spectra of FS

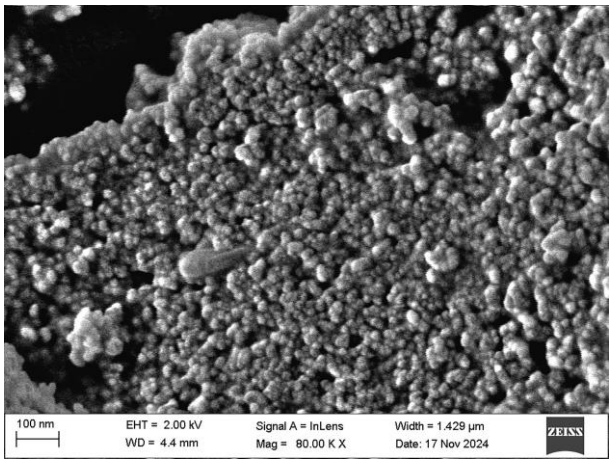

Fig. 2 SEM image of FS

2.2 Sample preparation

To ensure homogeneous dispersion of FS within the MOS cement matrix, the LBM and FS powders were first dry-mixed thoroughly before the gradual addition of the magnesium sulfate solution, followed by mechanical mixing. This mixing sequence was adopted to minimise FS agglomeration and promote uniform distribution throughout the paste. As shown in Fig. 2, FS particles exhibited a strong tendency to agglomerate owing to the presence of surface functional groups (Fig. 1(b)). Direct addition of FS into the salt solution could therefore result in local particle aggregation and non-uniform dispersion, whereas dry pre-mixing enabled intimate contact between FS and LBM particles, leading to a more homogeneous paste and improved reproducibility. The mix proportions were selected based on both previous studies and practical considerations. The molar ratios of MgO, $MgSO_4$ and H_2O were adopted from our previous work, in which the formation of the 5·1·7 phase and the corresponding mechanical performance of MOS cement were optimised [19]. Silicic acid contents ranging from 0 to 8 wt.% of LBM were previously reported to improve the mechanical properties of MOS cement [19]. However, the relatively high cost of silicic acid limits its practical application in large-scale production. In the present study, FS was selected as a more economically viable alternative. Unlike silicic acid, FS does not directly supply soluble silicate species but participates in the hydration process by consuming OH^-, thereby facilitating the formation of M-S-H gel and promoting microstructural densification. Since the optimum silicic acid dosage reported previously was below 5 wt.% of LBM [19], the FS dosage was selected in the range of 0–7 wt.% to determine whether a comparable or improved enhancement could be achieved while accounting for the different

157 reaction mechanism and reactivity of FS.

158 To isolate the influence of FS on the hydration behaviour and microstructural evolution of
159 MOS cement, all mixtures were prepared as cement pastes without the incorporation of sand or
160 other aggregates. Consequently, the system consisted only of LBM, FS, CA, and magnesium
161 sulfate solution, allowing the effects of FS on hydration, phase evolution, and mechanical
162 properties to be evaluated without interference from aggregate-related factors.

163 For the control specimen, the molar ratio of a-MgO to $MgSO_4 \cdot 7H_2O$ was maintained at 8.0,
164 and the molar ratio of $MgSO_4 \cdot 7H_2O$ to H_2O was fixed at 7:13. The FS proportion was varied in
165 increments of 2% by mass, beginning at 1% and increasing up to 7% of the LBM's weight, with
166 the corresponding sample codes of MOSFS2 (1% by mass FS), MOSFS3 (3% by mass FS),
167 MOSFS4 (5% by mass FS) and MOSFS5 (7% by mass FS). MOSFS1 without 0% FS was
168 designated as the control sample (see Table 2). Upon completion of a 120-second stirring period,
169 the slurry was placed into 40 mm cubic moulds and 40 × 40 × 160 mm^3 prismatic moulds,
170 yielding samples designated for strength evaluation, respectively. The samples underwent an
171 initial 24-hour cure at ambient temperature, after which they were demolded and moved to a
172 climate-controlled chamber set to 20 ± 2 °C and 60 ± 5% relative humidity for an additional 27 d
173 of sustained conditioning. Upon completion of the procedure, the specimens were removed and
174 placed in water at ambient temperature to assess their water resistance.

175

176 Table 2 Formulations of MOS cement pastes

Specimens	Molar ratios		FS	CA
	a-MgO/$MgSO_4$	$MgSO_4/H_2O$	(calculated based on the LBM weight)	
MOSFS1	8.0	0.35	-	0.5%
MOSFS2	8.0	0.35	1%	0.5%
MOSFS3	8.0	0.35	3%	0.5%
MOSFS4	8.0	0.35	5%	0.5%
MOSFS5	8.0	0.35	7%	0.5%

177

178 **2.3 Methods**

179 Specimen mechanical properties were measured per the GB/T 17671-2021, employing an
180 electronic servo testing apparatus (CMT5105). The values of strength were drawn from the

average of six samples. X-ray diffraction (XRD) was employed to conduct the phase composition, using an AL-Y3500 diffractometer operated from 5° to 80° 2 theta with a step interval of 0.02° and a scanning speed of 0.03 s/step. Solid-state ^{29}Si NMR spectra were acquired on a Bruker 400M spectrometer. SU8600 (SEM) was acquired to investigate the micromorphology and elemental composition of the hydration products in MOS cement. Lattice spacing of the hydration products was measured using high-resolution transmission electron microscopy (TEM, Talos 200S). Thermal stability of the hydration products was evaluated with a thermal analyser (TG-DSC, SDT 650) under argon, applying a heating ramp of 5 °C/min over the temperature span of 45–1100 °C. The pore structure of cement was evaluated via mercury intrusion porosimetry using a Micromeritics Autopore V 9605. Elements' binding energy was analysed using an AXIS SUPRA+ (XPS), with the binding energy scale referenced to the C 1s peak at 284.8 eV.

3 Results

3.1 Strengths

As illustrated in Fig. 3, the strengths of MOS cement blended with FS were measured at multiple curing ages. The MOS cement's compressive strength increased with age owing to the influence of FS. The compressive strength of MOSFS5 reached 45.5 MPa after 1 d of air curing, which was 28.5% greater than that of the reference sample MOSFS1. By day 7, the compressive strength of MOSFS5 had surpassed the control's value by 23.2%, with this particular blend yielding the peak result in both comparisons. MOS cement's compressive strength also grew with FS addition, which was especially effective in promoting early-age strength gain. After 28 d of curing, MOSFS4's compressive strength achieved the highest value (78.8 MPa), exceeding MOSFS5 and MOSFS1 by 2.5% and 19.7%, respectively. Blending FS into MOS cement preparation contributed favourably to the progression of its compressive strength. Flexural strength changes in MOS cement exhibited a pattern like that of compressive strength. FS served as a crucial factor in promoting the short-term flexural strength development of cement. The 28-d flexural strength reached a maximum of 18.9 MPa for MOSFS4, representing a 34.1% improvement over MOSFS1. FS contributed substantially to the performance enhancement of MOS cement.

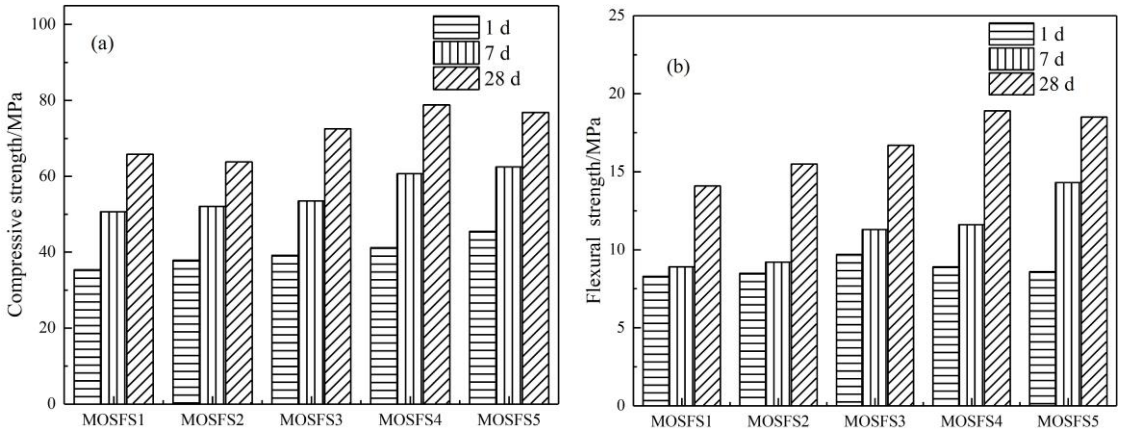

Fig. 3 Strengths of cement: (a) compressive strength; (b) flexural strength

3.2 Phase composition

The X-ray diffraction results of MOS cement following air curing over a range of time periods are displayed on Fig. 4. In comparison to Fig. 1(a), significant diffraction peaks corresponding to FS are absent in Fig. 4, likely due to the limited FS content in the MOS cement matrix, potential FS involvement in the hydration process leading to its depletion, or a combination of both. The observed diffraction peaks of calcite suggested its presence in the MOS cement matrix, likely stemming from the raw material used in the manufacturing of LBM. Fig. 4(a) demonstrates that the peaks at $2\theta = 37.33°$, 17.80°, and 9.44°, attributed to the (222), (200), and (-101) planes of the 5·1·7 phase (reference code: 04-019-9611), exhibited no significant discrepancy. However, the peak intensity at $2\theta = 36.75°$, corresponding to the (-206) crystal plane of the 5·1·7 phase, evolved with greater FS additions to the MOS cement matrix. Application of the Scherrer equation [20] (Scherrer constant = 0.943, X-ray source wavelength = 0.154056 nm) to the (-206) crystal plane yielded crystallite sizes of 32.89, 33.12, 32.99, and 31.27 nm for the 5·1·7 phase in the MOSFS1, MOSFS2, MOSFS4, and MOSFS5 systems, respectively. Quantitative analysis of Fig. 4(a) showed that FS inclusion contributed to somewhat enhanced growth of the 5·1·7 phase along the (-206) plane. The MOS cement, cured for 28 d, showed $Mg(OH)_2$ (reference code: 01-071-5972) crystallite sizes at the (011) plane ($2\theta = 37.97°$) of 22.35, 25.15, 21.94, and 20.96 nm, corresponding to MOSFS1, MOSFS2, MOSFS4, and MOSFS5, respectively. Furthermore, the size of 5·1·7 phase crystallites corresponding to the (222) plane was determined to be 44.62, 45.80, 43.12, and 42.18 nm, respectively. No persistent increase in the $Mg(OH)_2$ crystallite size at the (011) plane was observed as the FS content in the MOS cement

matrix was elevated. Similarly, no appreciable growth was observed in the crystallite dimensions of the 5·1·7 phase on the (222) plane. Additionally, the 5·1·7 phase within the matrix contributed significantly to the strength development, exerting a critical influence on the engineering behaviour of cement. In line with the mechanical property variations presented in Fig. 3, this implies that FS contributes to cement hydration, possibly assisting the existence of a new phase.

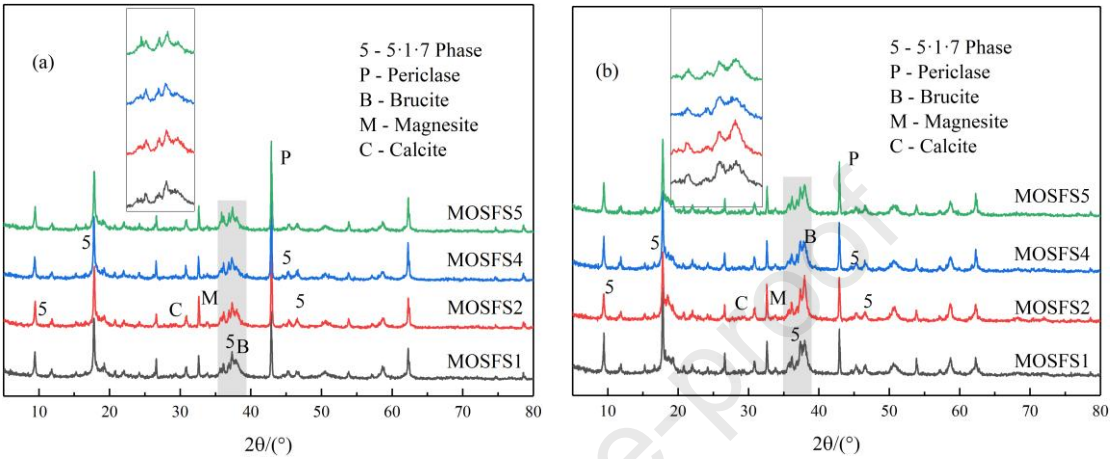

Fig. 4 XRD patterns (a)1 d; and (b) 28 d

The TG-DTG results for MOS cement blended with FS are depicted in Fig. 5. The weight loss of MOSFS1, MOSFS2, and MOSFS4 after 1 d of curing was 32.93%, 32.87%, and 31.79%, respectively. After 28 d, it increased to 34.88%, 34.20%, and 33.81%, respectively. As curing continued, the mass loss of the MOS cement also increased, indicating the generation of hydration products during the curing process. Compared to the mass loss observed in the control sample MOSFS1, which did not contain FS, the addition of FS resulted in a reduction in hydration products in both MOSFS2 and MOSFS4. Within the matrix, the decomposition temperatures of the 5·1·7 phase are shown in schemes (1) to (2) [21,22].

$$5Mg(OH)_2 \cdot MgSO_4 \cdot 7H_2O \rightarrow 5Mg(OH)_2 \cdot MgSO_4 + H_2O \qquad \sim 200\ ^\circ C \qquad (1)$$

$$5Mg(OH)_2 \cdot MgSO_4 \rightarrow MgO + MgSO_4 + H_2O \qquad 300 \sim 450\ ^\circ C \qquad (2)$$

Prominent peaks were identified at approximately 405 °C, indicative of the decomposition of $Mg(OH)_2$, and at around 430 °C, which is connected with the loss of water from the compound $5Mg(OH)_2 \cdot MgSO_4$. The peaks appeared at temperatures above 500 °C, attributed to the presence of $MgCO_3$ and $CaCO_3$ introduced by the raw materials. The peak shift observed near 405 °C in Fig. 5(a) implies a decreased $Mg(OH)_2$ content in the FS-modified MOS cement, most notably in MOSFS4. FS, when added to the MOS cement manufacturing process, exhibited the potential to

restrain $Mg(OH)_2$ generation at the early hydration stage. As shown by the DTG curves, a change at roughly 430 °C points to the fact that FS did not contribute to any substantial growth in the creation of $5Mg(OH)_2 \cdot MgSO_4$. This further suggests that the concentration of the 5·1·7 phase did not significantly rise (see DTG curves of MOSFS2) and may have even decreased due to the introduction of FS (see DTG curves of MOSFS4). Unlike Fig. 5(a), Fig. 5(b) presents DTG curves with a noticeable change around 405 °C, demonstrating that the $Mg(OH)_2$ content in the hydration products elevated as curing advanced, stemming from the continued hydration of remaining MgO. However, the DTG curve of MOSFS4 indicated that the $Mg(OH)_2$ content was lower than that in MOSFS1, likely due to the excess content of FS, which continued inhibiting $Mg(OH)_2$ formation. The proportion of $Mg(OH)_2$ was correlated to the FS dosages in MOS cement. Additionally, the change in $5Mg(OH)_2 \cdot MgSO_4$ content, obtained from the DTG data at approximately 430 °C, indicated that FS negatively affected the generation of the 5·1·7 phase. The M-S-H gel (see Figs. 6 and 8) had an impact on the loss in mass within the 45–200 °C; meanwhile, the alteration in the DTG profiles due to the breakdown of $5Mg(OH)_2 \cdot MgSO_4$ signified a fluctuation in the amount of the 5·1·7 phase.

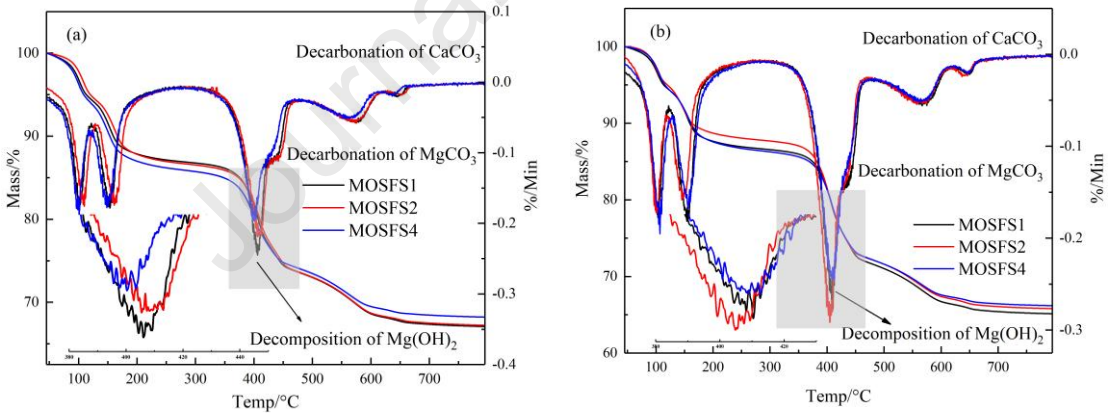

Fig. 5 TG-DTG curves of MOS cement containing FS after curing for (a) 1 d; and (b) 28 d

3.3 NMR

Fig. 6 displays the ^{29}Si NMR spectra of MOS cement with FS, cured in air for various periods. As curing progresses, the ^{29}Si peaks, reflecting the diverse chemical environments of Si atoms, undergo distinct changes. Q^n represents multiple types of silicon-oxygen tetrahedra [23,24]. As illustrated in Fig. 6, the calcium silicate hydrate structure features Q^1, Q^2, Q^3, and Q^4 representing the end-group silicate tetrahedron, the chain-type unit, the layered or branched-chain configuration, and the three-dimensional network arrangement, respectively [25,26]. In the

components used to produce MOS cement, there were no silicate minerals (e.g., tricalcium silicate, dicalcium silicate), indicating that the peaks of Q^n are not associated with calcium silicate hydrate gel. Additionally, the characteristic peak of the M-S-H gel, Q^{3b}, appeared at around 94.0 ppm in Fig. 6 [19,27,28]. During the fabrication of MOS cement, the detected Q^4 peaks corresponded to the addition of FS, which exists primarily in its amorphous form (see Fig. 1(a)). The presence of calcium silicate hydrate cannot explain variations in peak behaviour over the curing period. The presence of FS strongly stimulated the creation of M-S-H gel in the cement system.

Table 3 presents the ^{29}Si chemical shift values (ppm) along with their respective peak intensities (%) for MOSFS4. Over the course of curing, the relative peak intensities of Q^4 diminished, suggesting that FS was gradually consumed throughout curing. Q^2 peaks pointed to the chain-like organisation within the M-S-H gel, while Q^3 revealed its layered form [29]. The peaks at Q^{3a} were attributed to a serpentine-type (T:O) structure within the M-S-H gel. On the other hand, the peaks identified at Q^{3b} and Q^{3c} pointed to a structural arrangement more reminiscent of talc (T:O:T) [30,31]. Using the $I(Q^3)/I(Q^2)$ intensity ratio, the relative proportions of layered (Q^3) and chain-like (Q^2) M-S-H gel structures were assessed. Scheme (3) was employed to determine the degree of polymerisation of the M-S-H gel [23,28,32]

$$CD = [3I(Q^{3b})+3I(Q^{3a})+2I(Q^2)+I(Q^1)]/3[3I(Q^{3b})+3I(Q^{3a})+I(Q^2)+I(Q^1)] \quad (3)$$

After 1, 7, and 28 d of curing, the M-S-H gel in MOSFS4 exhibited $I(Q^3)/I(Q^2)$ ratios of 1.09, 2.14, and 0.91, and polymerisation degrees of 0.75, 0.83, and 0.72, respectively, pointing to a change in the layered M-S-H gel content as curing progressed. Cleavage of the Si-O-Si bond in the silicon-oxygen tetrahedron resulted in a decrease in $I(Q^3)/I(Q^2)$ [19]. In the MOS cement matrix, the M-S-H gel structure tended to transition into a chain-like form, suggesting that the layer M-S-H gel structure within the MOS cement exhibited lower stability compared to the chain-like M-S-H gel. Additionally, as curing continued, $I(Q^{3c})$ also increased, suggesting that the M-S-H gel structure with talc (T:O:T) became more pronounced. FS participated in the MOS hydration and enhanced the generation of M-S-H gel. Figs. 4 and 5 collectively indicate that FS had a detrimental impact on 5·1·7 phase growth, but the FS-containing samples demonstrated a beneficial influence on strength development, which points to the crucial contribution of M-S-H gel to the hardening of cement.

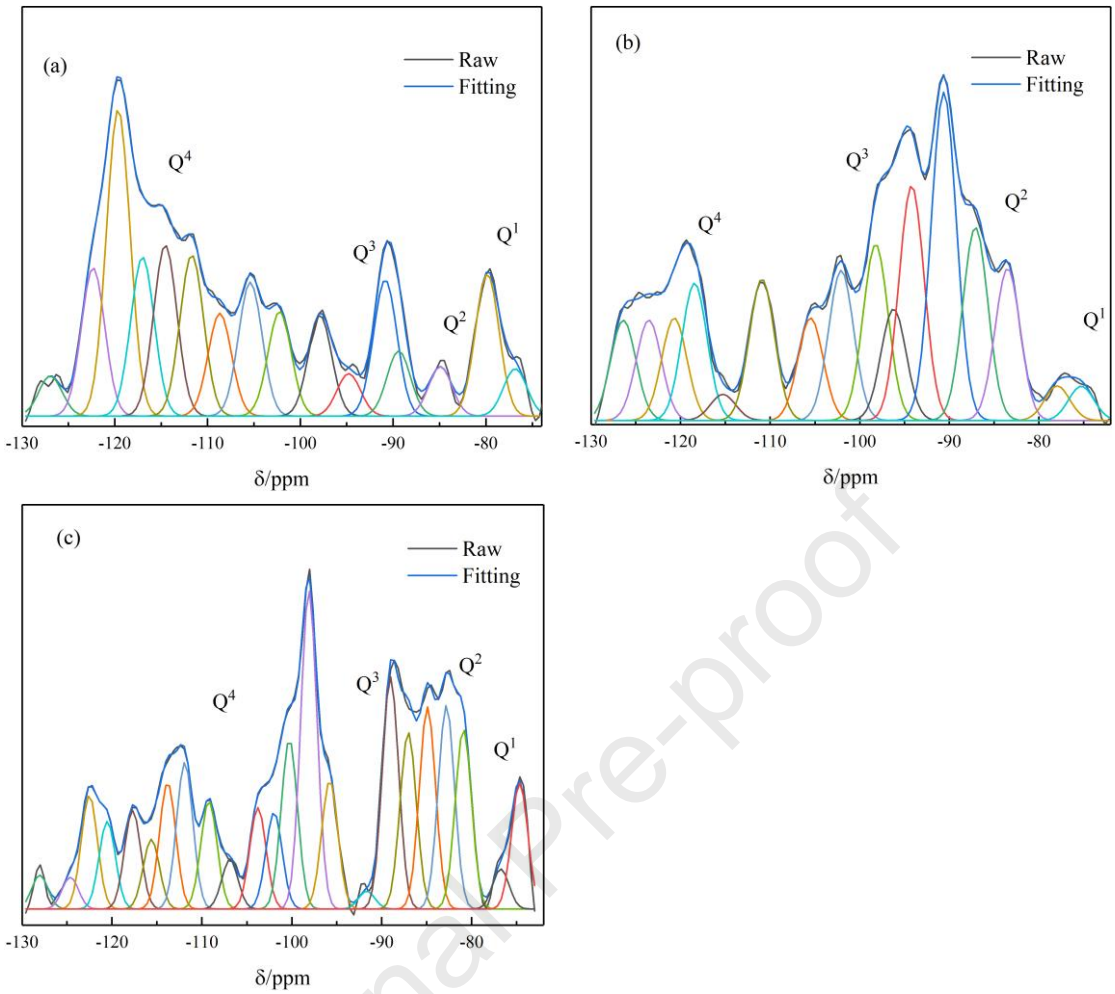

303 Fig. 6 ^{29}Si NMR spectra of MOSFS4 cured in air for (a) 1 d; (b) 7 d; and (c) 28 d

304 Table 3 Relative ^{29}Si chemical shifts (ppm) and peak intensities (%) of MOSFS4 cured in air for

305 various periods

Specimens	Q^1		Q^2		Q^{3a}		Q^{3b}		Q^{3c}		Q^4	
	Center	Area	Center	Area	Center	Area	Center	Area	Center	Area	Center	Area
MOSFS4 (1 d)	-76.84	2.48	-84.92	13.42	-90.84	7.13	-94.77	2.23	-97.87	5.27	-119.62	69.48
MOSFS4 (7 d)	-76.82	3.23	-83.67	16.24	-90.61	15.43	-94.20	11.04	-98.22	8.29	-119.27	45.77
MOSFS4 (28 d)	-76.75	5.81	-84.73	26.66	-90.03	8.73	-95.77	4.49	-98.10	11.15	-111.91	43.16

306

307 **3.4 Pore structure**

308 The pore structure of cement is depicted in Fig. 7, while the corresponding pore size
309 distribution is shown in Fig. 7(a). The porosity of MOSFS1, MOSFS2, and MOSFS4 was 33.87%,
310 29.12%, and 25.60%, respectively, while the average pore sizes of MOSFS1, MOSFS2, and
311 MOSFS4 were 53.82, 38.73, and 36.03 nm, respectively. MOSFS4 exhibited the highest gel pore

content (< 10 nm) of 6.05%, compared to MOSFS1 and MOSFS2 (see Fig. 7(c)). FS significantly lowered the porosity of the MOS cement and enhanced the generation of supplementary gel pores. To some extent, the proportion of such pores indicated the quantity of gel formed in the binder system [20]. The results show that the proportions of pores smaller than 50 nm in MOSFS1, MOSFS2, and MOSFS4 are 31.87%, 45.52%, and 47.72%, respectively. In contrast, the proportions of pores larger than 50 nm decrease correspondingly with increasing FS dosage. In cement-based materials, pores smaller than 50 nm generally have a limited adverse effect on mechanical properties and are commonly associated with a denser hydration product network, whereas pores larger than 50 nm act as preferential pathways for crack propagation and water ingress, thereby reducing both mechanical performance and water resistance.

The increase in the proportion of pores smaller than 50 nm, together with the corresponding reduction in larger pores, indicates that the incorporation of FS effectively refines the pore structure and promotes microstructural densification. This pore refinement contributes not only to the improvement of compressive strength but also to the enhanced water resistance of MOS cement by reducing the connectivity of capillary pores and limiting water penetration.

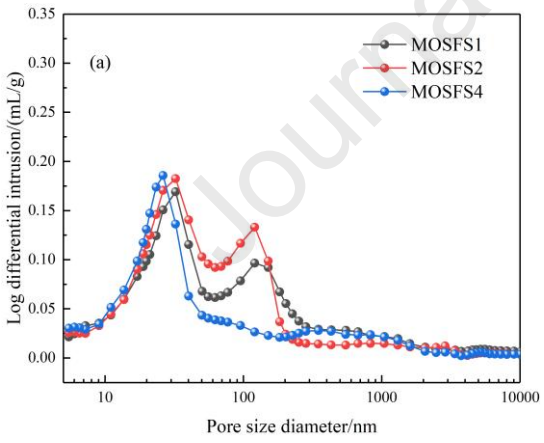

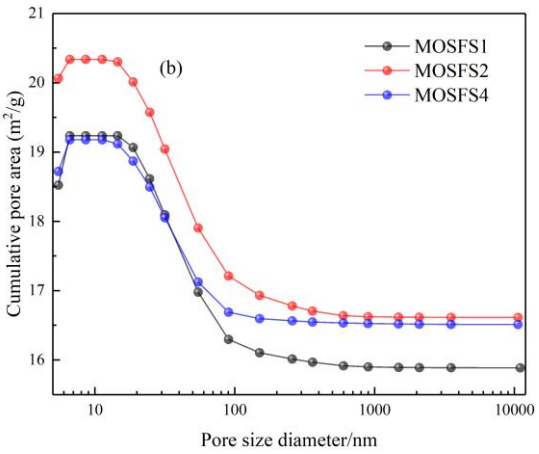

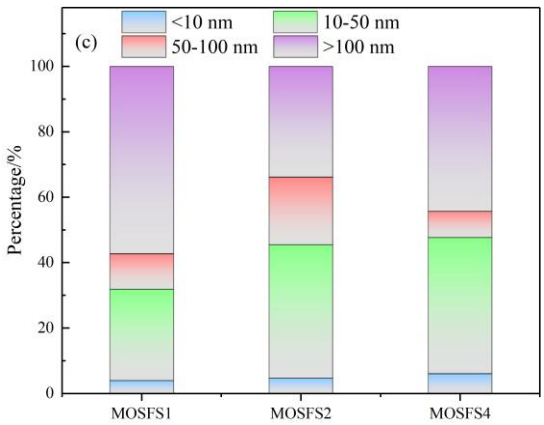

Fig. 7 Pore structure of MOS cement: (a) pore size distribution; (b) pore area; (c) pore contents with different sizes

3.5 XPS

As depicted in Figs. 8 and 9, the XPS data of FS-bearing MOS cement were obtained after curing for varying lengths of time. In Fig. 8(a), the peaks located at 1303.47, 1304.63, and 1305.72 eV were identified as MgO/Mg-OH, Mg-SO_4, and Mg-CO_3, respectively [34,35]. Fig. 8(c) depicts the Si 2p spectral features, linked to SiO_2, which result from incorporating LBM into the MOS cement during production (see Table 1). The contribution from additional FS was also reflected in the Si 2p peaks in Fig. 9. However, in Figs. 9(b) and 9(d), a new Mg 1s peak was observed, indicating the generation of new chemical bonds involving Mg^{2+} during the curing process of cement. A similar pattern was also noted in Fig. 9(e), with the emergence of a new Si 2p peak. In comparison to Fig. 8, the observed shifts in the Mg 1s and Si 2p peaks offered a hint of the formation of a compound between Mg^{2+} and Si^{6+}. Such findings gave indirect backing to what was observed in Fig. 6, namely that M-S-H gel was produced within the hardened cement. In Figs. 9(c) and 9(e), the areas of the Si 2p peaks at 101.75 eV and 101.97 eV accounted for 19.48% and 32.72%, respectively. The rise in new peaks demonstrated that prolonged curing led to increased FS involvement in the hydration of MOS cement, which promoted M-S-H gel formation, aligning with the trend observed in Fig. 6. As shown by comparing Fig. 8(b) and Fig. 9(d), increased FS concentration in the cement brought about a decline in the Mg 1s binding energy, together with a shift of the Si 2p binding energy toward lower values. This effect was ascribed to the elevated M-S-H gel content, as reflected by the comparatively greater binding energies of Mg 1s and Si 2p shown in Figs. 9(b) and (c). FS consumption during the MOS cement curing process triggered changes in the M-S-H gel content, subsequently resulting in variations in the binding energy of Mg 1s and Si 2p.

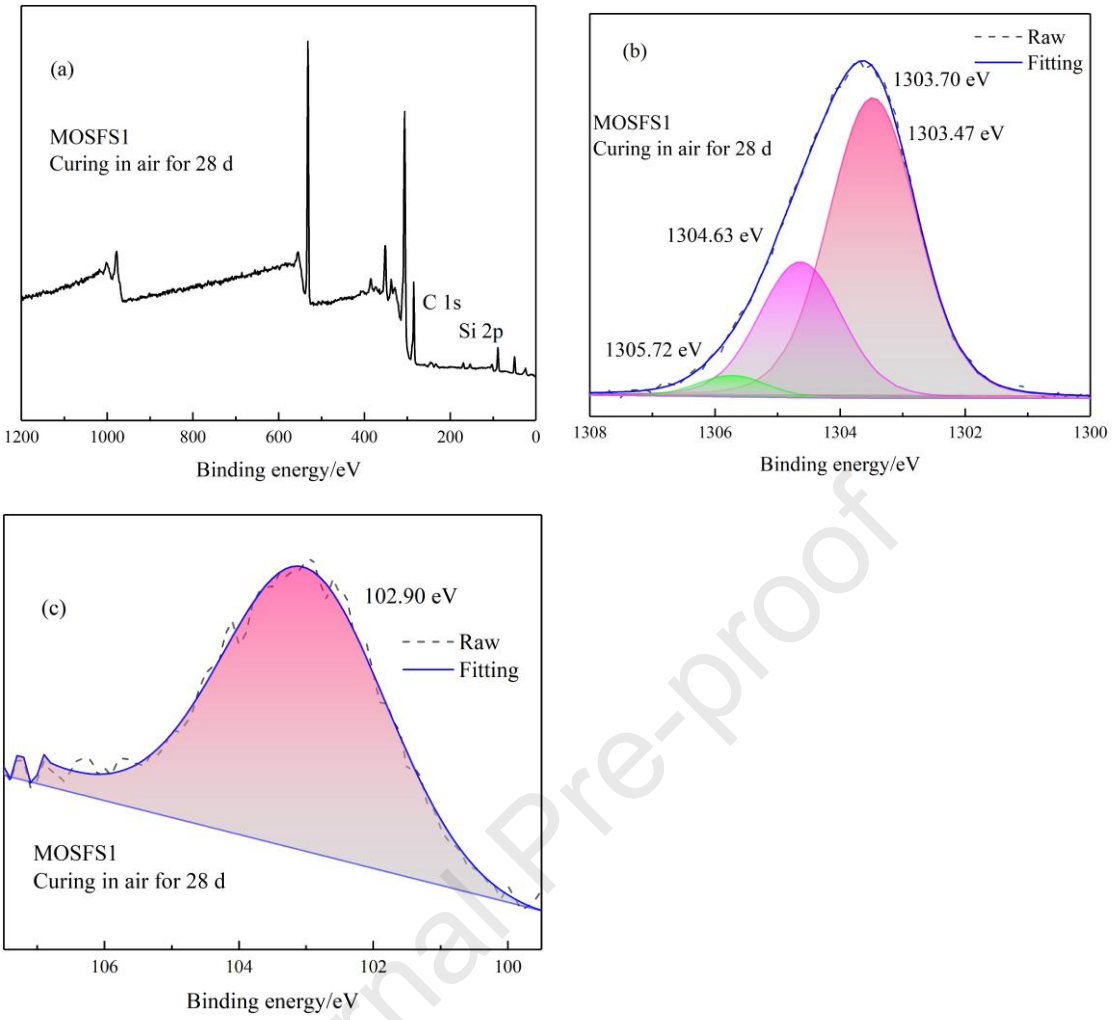

351 Fig. 8 XPS data of MOSFS1: (a) XPS spectra; (b) Mg 1s; (c) Si 2p

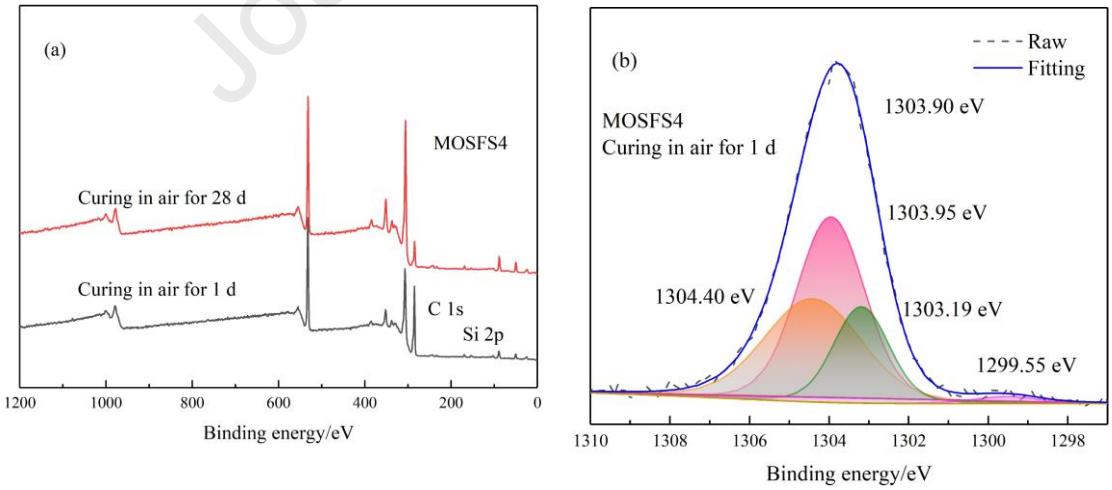

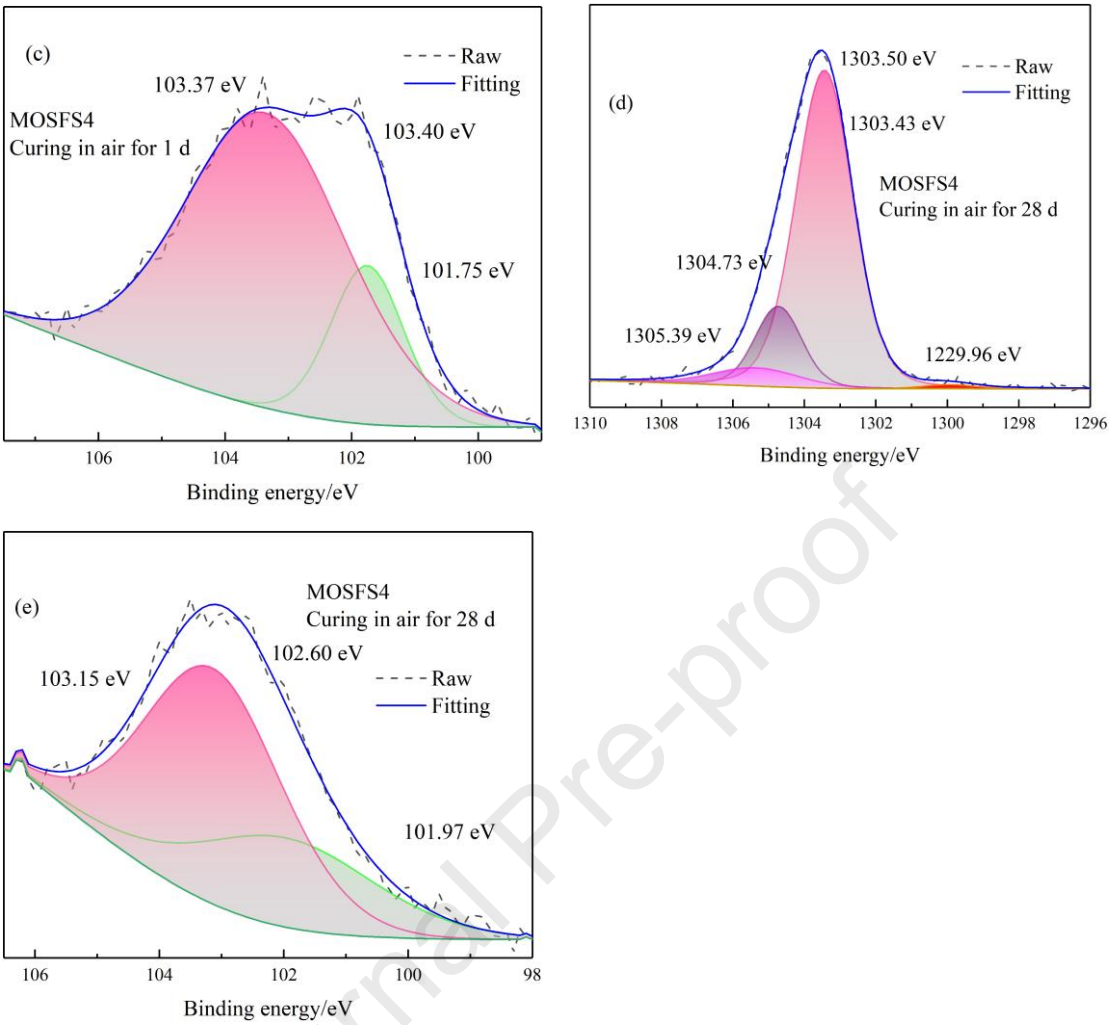

352 Fig. 9 XPS data of MOSFS4: (a): XPS spectra; (b), (d): Mg 1s; (c), (e): Si 2p

353

354 **3.6 SEM and HR-TEM**

355 The SEM images in Fig. 10 depict MOS cement following 28 d of curing in air. The crystals
356 visible at Points 1 (illustrated in Fig. 10(a)) and 5 (illustrated in Fig. 10(b)) were assigned to the
357 5·1·7 phase according to their elemental composition from EDS and their morphology. Plate-like
358 crystals were observed at Points 2, 3, and 4, exhibiting an elemental ratio similar to that of the
359 5·1·7 phase, as presented by the EDS results. However, these plate-like crystals exhibited a
360 different morphology compared to the 5·1·7 phase, more closely resembling the morphology of
361 the $3Mg(OH)_2 \cdot MgSO_4 \cdot 8H_2O$ phase, which was also characterised by a plate-like structure [36].
362 The presence of weak acids during MOS cement production caused the $3Mg(OH)_2 \cdot MgSO_4 \cdot 8H_2O$
363 phase to convert into the 5·1·7 phase, which consequently became the dominant strength-bearing
364 component in the matrix [19]. According to the EDS results, the plate-like crystals could not be

identified as the $3Mg(OH)_2 \cdot MgSO_4 \cdot 8H_2O$ phase. Instead, they were more likely a form of basic magnesium sulfate whisker, distinct from the 5·1·7 phase, described by the formula $aMg(OH)_2 \cdot bMgSO_4 \cdot cH_2O$. Fig. 10(c) shows that Si exhibited a homogeneous dispersion across the MOS cement matrix surface, as indicated by element mapping. The observation of silicon on the 5·1·7 phase surface at Point 5 further suggests FS involvement in the matrix structure's formation, as shown in Fig. 7. In contrast to Fig. 10(c), Fig. 10(d) showed an area where element Si was enriched, which differed from the distribution observed in Fig. 10(c), suggesting that the partial FS introduced into the MOS cement was not uniformly distributed throughout the matrix. The relative element ratios at Points 6 and 7 exhibited a significant difference in Si content. Comparison of the EDS results from Points 6, 7, and 8 (see Fig. 10(e)) suggested that this difference was likely due to the presence of forsterite, which was derived from the LBM produced by the calcination of magnesite. The EDS results, presented in Figs. 10(f) and 10(g), reveal similar relative element ratios of Si, suggesting that the presence of Si was consistent and not incidental, whether on the crystal surfaces (Points 9 and 11) or the gel-like surfaces (Points 10 and 12). Given the findings presented in Fig. 6, the silicon detected on the crystalline and gel-like surfaces resulted from the generation of M-S-H gel. Additionally, the M-S-H gel absorbed on the surface of the 5·1·7 phase provided further insights into the influence of FS on the crystal growth of the 5·1·7 phase (see Fig. 4). By integrating Fig. 7 with Figs. 10(c) and 10(f), the formation of M-S-H gel within the pores and matrix of the MOS cement was observed, which contributed to enhancing its densification.

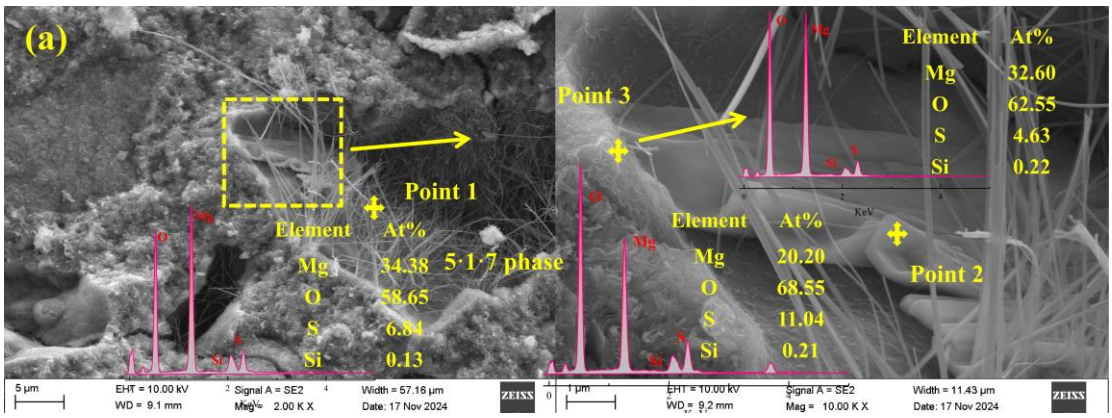

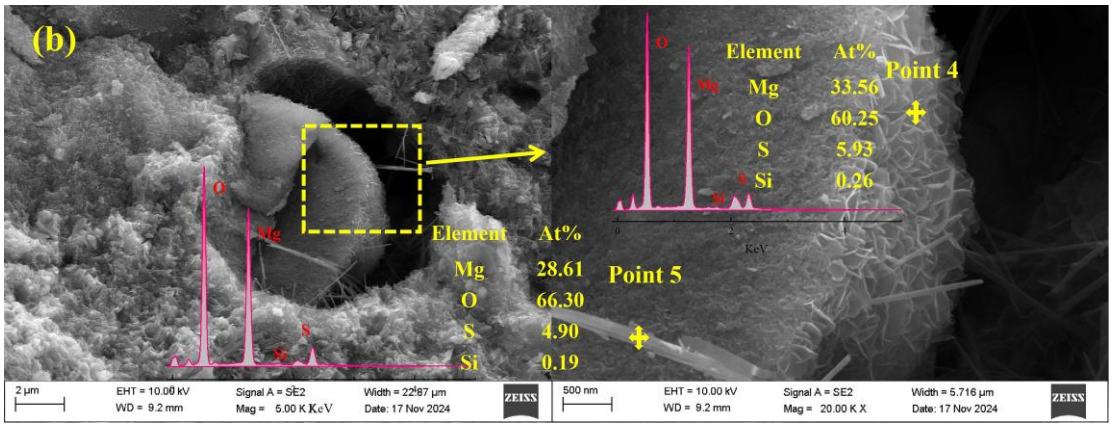
(b)
O
Mg
S
Si
Element At%
Mg 28.61
O 66.30
S 4.90
Si 0.19
Point 5
Element At%
Mg 33.56
O 60.25
S 5.93
Si 0.26
Point 4
KeV
2 μm
EHT = 10.00 kV
WD = 9.2 mm
Signal A = SE2
Mag = 5.00 K KeV
Width = 22.87 μm
Date: 17 Nov 2024
ZEISS
500 nm
EHT = 10.00 kV
WD = 9.2 mm
Signal A = SE2
Mag = 20.00 K X
Width = 5.716 μm
Date: 17 Nov 2024
ZEISS

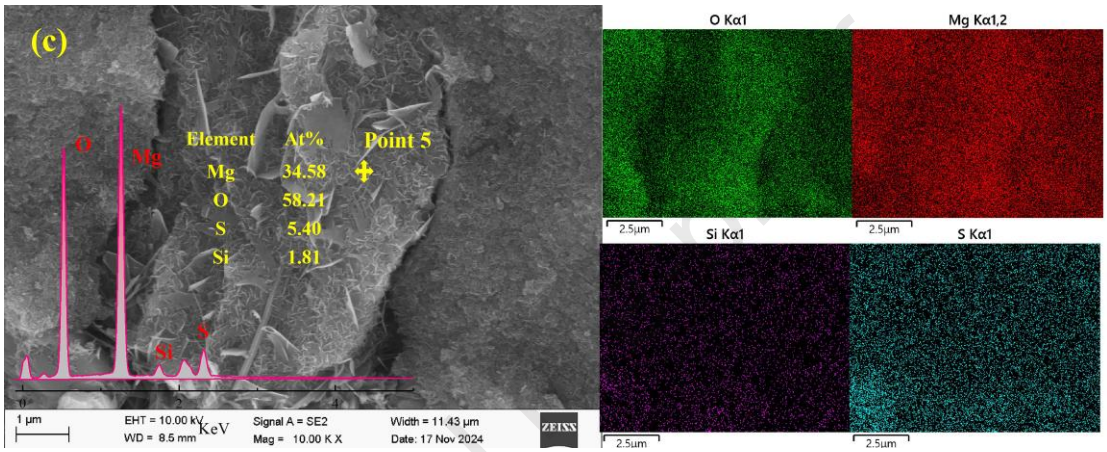
(c)
O
Mg
S
Si
Element At%
Mg 34.58
O 58.21
S 5.40
Si 1.81
Point 5
KeV
1 μm
EHT = 10.00 kV
WD = 8.5 mm
Signal A = SE2
Mag = 10.00 K X
Width = 11.43 μm
Date: 17 Nov 2024
ZEISS
O Kα1
Mg Kα1,2
Si Kα1
S Kα1
2.5μm

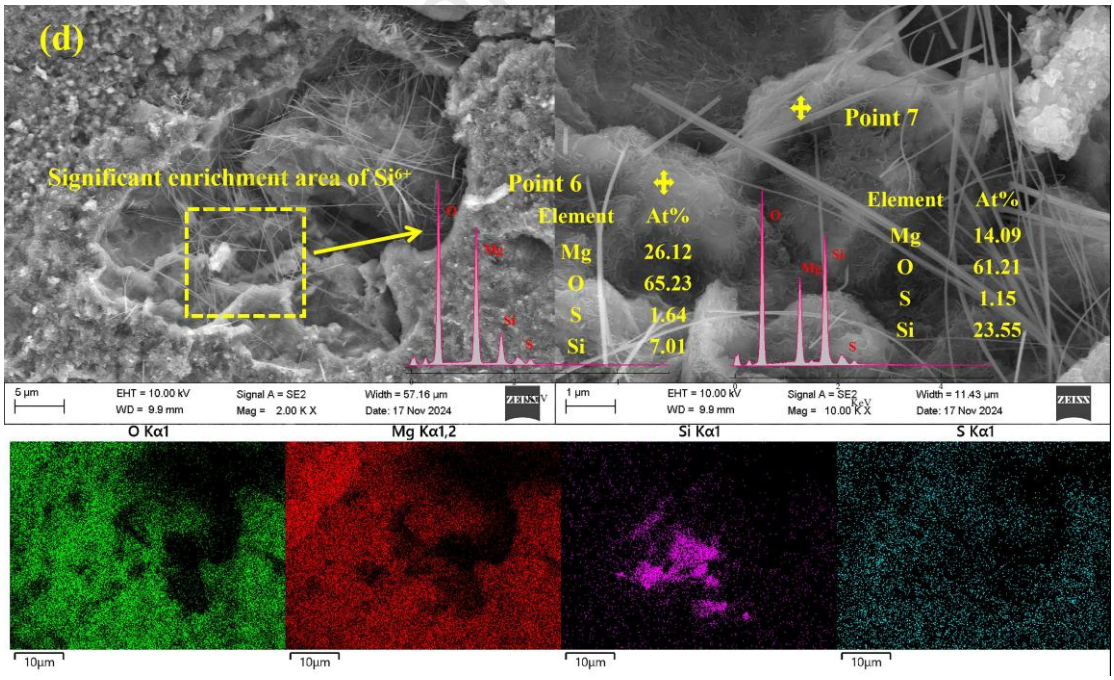
(d)
Significant enrichment area of Si6+
Point 6
Element At%
Mg 26.12
O 65.23
S 1.64
Si 7.01
Point 7
Element At%
Mg 14.09
O 61.21
S 1.15
Si 23.55
5 μm
EHT = 10.00 kV
WD = 9.9 mm
Signal A = SE2
Mag = 2.00 K X
Width = 57.16 μm
Date: 17 Nov 2024
ZEISS
1 μm
EHT = 10.00 kV
WD = 9.9 mm
Signal A = SE2
Mag = 10.00 K X
Width = 11.43 μm
Date: 17 Nov 2024
ZEISS
O Kα1
Mg Kα1,2
Si Kα1
S Kα1
10μm

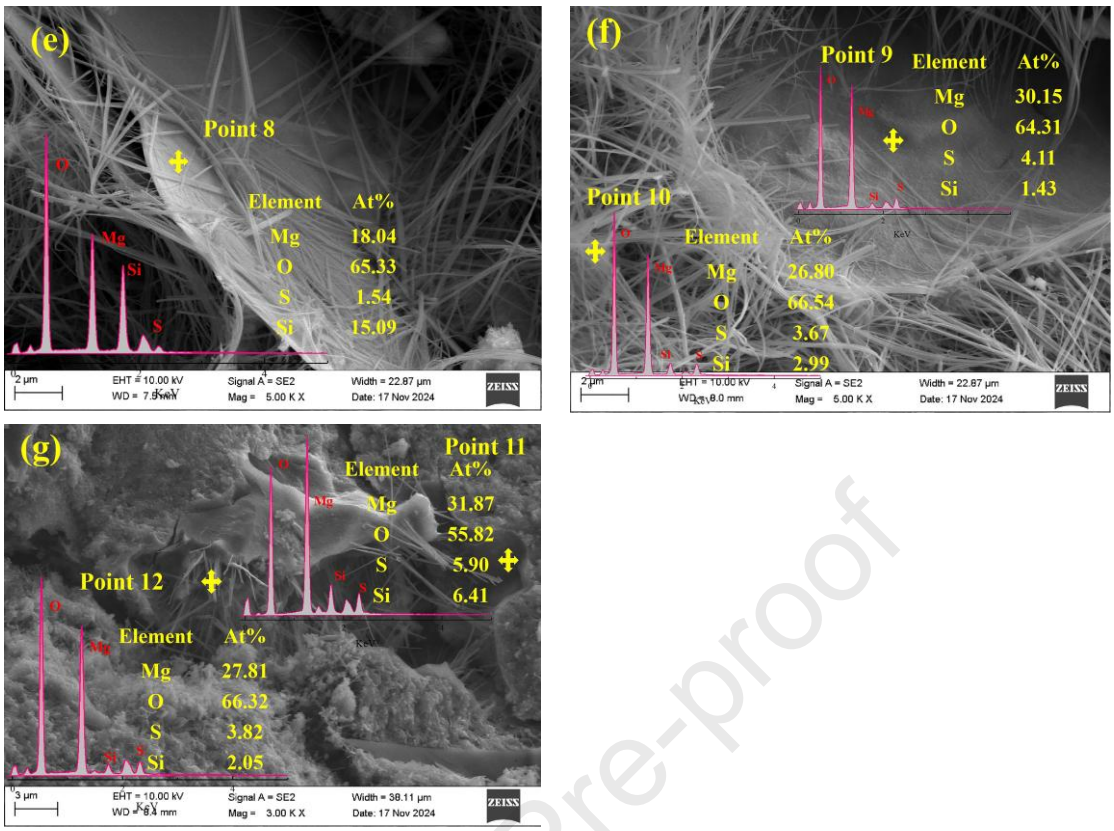

385 Fig. 10 SEM images: (a), (b): MOSFS1; (c), (d): MOSFS2; (e), (f), (g): MOSFS4

386 The HR-TEM images in Fig. 11 depict MOSFS4. Elemental mapping and d-spacing
387 evaluation indicated that the lattice spacing of the observed particles matched the 5·1·7 phase at
388 the (222) plane, verifying their classification as this phase. No appreciable variation in the
389 interplanar distance of the 5·1·7 crystal was observed upon introducing FS into MOS cement.
390 Additionally, element mapping revealed an area of Si enrichment that was located close to the
391 5·1·7 crystal. The behaviour captured in Fig. 11 mirrored observations from Figs. 10(f) and 10(g),
392 wherein silicon was identified on the 5·1·7 crystal's surface. This elemental enrichment reinforced
393 the notion that M-S-H gel had partially gathered on the 5·1·7 phase, a result attributable to FS
394 engaging in the hydration reactions of MOS cement.

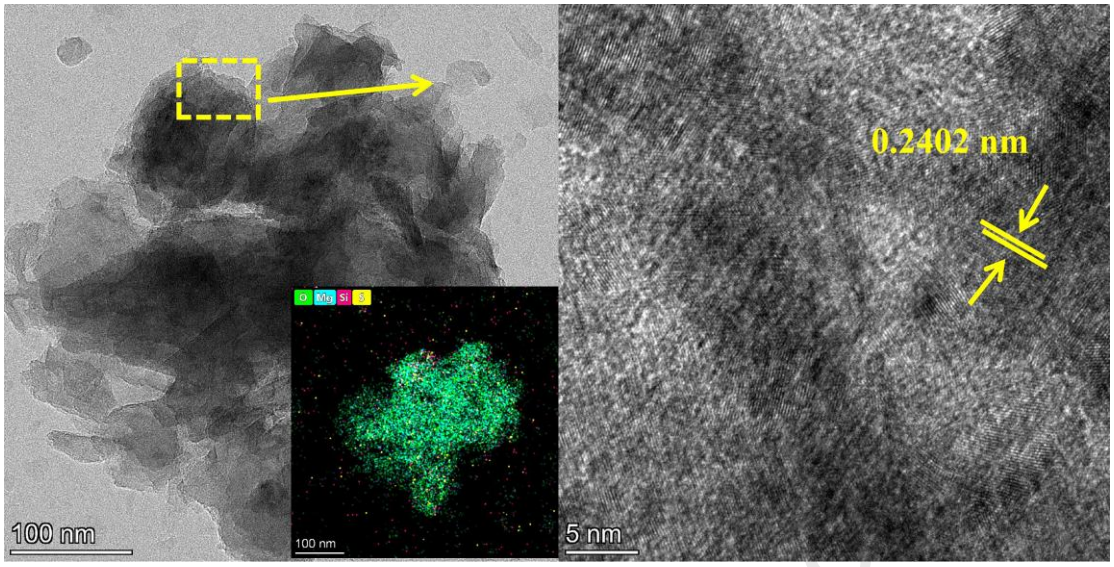

Fig. 11 HR-TEM image of MOSFS4

3.7 Water resistance

The compressive strength and TG-DTG curves of water-immersed MOS cement are presented in Fig. 12. Upon 14 d of submersion, the strength values were 45.8 MPa for MOSFS1 and 55.1 MPa for MOSFS4, marking a 20.30% enhancement (see Fig. 12(a)). With water immersion duration extended to 90 d, the compressive strengths of MOSFS1 and MOSFS4 were 32.6 and 57.3 MPa, respectively, with MOSFS4 exhibiting a 75.76% higher compressive strength than MOSFS1. Moreover, the compressive strength of MOSFS5, at 54.3 MPa, was lower than that of MOSFS4. An increase in the FS dosage in MOS cement did not result in an enhancement of its compressive strength. As curing continued, the benefits of FS positively influencing the evolution of compressive strength became more obvious. Fig. 12(b) shows the mass change data of cement after 90 d of water immersion. Mass losses of MOSFS1, MOSFS2, and MOSFS4 were 35.37%, 35.86%, and 35.96%, respectively. The shift in the DTG curves around 430 °C indicates a lower content of $5Mg(OH)_2 \cdot MgSO_4$ in the MOS cement containing FS. Additionally, the greater loss observed from MOSFS2 and MOSFS4 between 45 °C and 200 °C, compared to MOSFS1, suggests a higher amount of water loss within this temperature range. The DTG curve profile of MOS cement recorded between 45 and 200 °C corresponds to the dehydration of bound water from the 5·1·7 phase (scheme 1 in section 3.2). Analysis of the DTG curves, specifically the changes observed between 45 °C and 200 °C and around 430 °C, indicates that FS contributed to the reduction of the 5·1·7 phase (see Fig. 5). The contribution of M-S-H gel to the mass change of

cement across the 45–200 °C region also provided circumstantial evidence for its occurrence within the hardened matrix. Heating the M-S-H gel led to a pronounced mass loss from 45 to 200 °C, primarily because of water existing in the gel, which existed in adsorbed or bound forms [24,37-39]. The decomposition of M-S-H gel occurred within the temperature range of 440 to 650 °C [23,24]. However, the DTG signals assigned to M-S-H gel in the 45–200 °C range displayed only one distinct peak. The evidence from Figs. 10(f) and 10(g), together with the reduced proportion of the 5·1·7 phase in MOSFS1 indicated by the mass loss comparison between Fig. 5(b) and Fig. 12(b) over the 45–200 °C interval, leads to the conclusion that the surficial M-S-H gel provided a certain protective function. Meanwhile, as shown by the DTG curves between 45 and 200 °C, the amount of M-S-H gel was more pronounced in MOSFS4 compared with the other two specimens. The DTG curves at approximately 405 °C revealed that MOS cement incorporating FS contained less $Mg(OH)_2$ than MOSFS1. Even after water immersion, the additive effectively suppressed brucite formation, thereby improving the material's water resistance. This variation in hydroxide content underscored the favourable influence of FS on the engineering performance of the cementitious system.

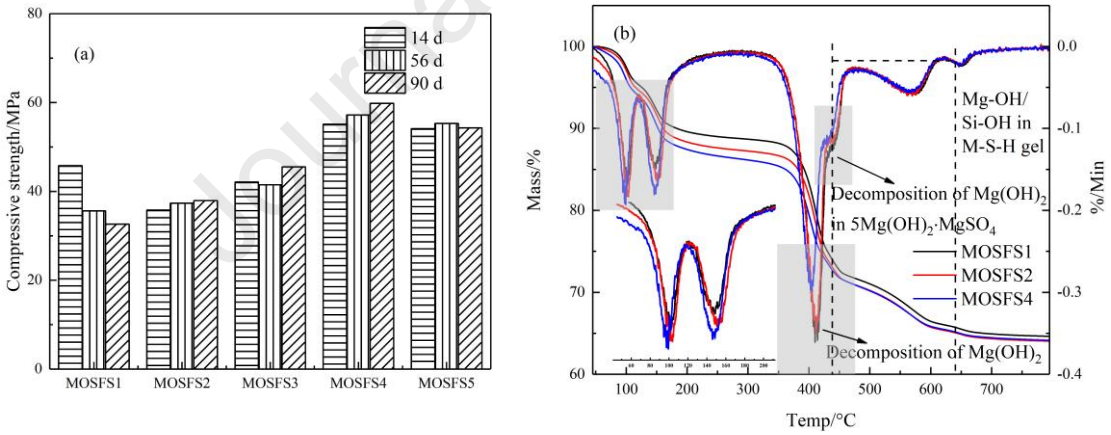

Fig. 12 Compressive strength and TG-DTG curves of cement: (a) compressive strength; (b) TG-DTG curves

Fig. 13 displays the XPS spectra of MOSFS4 following 90 d of immersion in water. A fresh peak at 1299.96 eV emerged in Fig. 13(a), mirroring the behaviour noted in Fig. 9, which implies that FS had an impact on the hydration product composition. The peak at 103.91 eV in Fig. 13(c) was attributed to Si-O. The proportion of the Si 2p peak located at 102.47 eV reached 61.24%, surpassing the corresponding value in Fig. 9, which suggests that the new phase continued to

evolve after the cement was submerged in water. Combining the Si 2p and NMR spectra, the continuous consumption of FS during the curing period was confirmed.

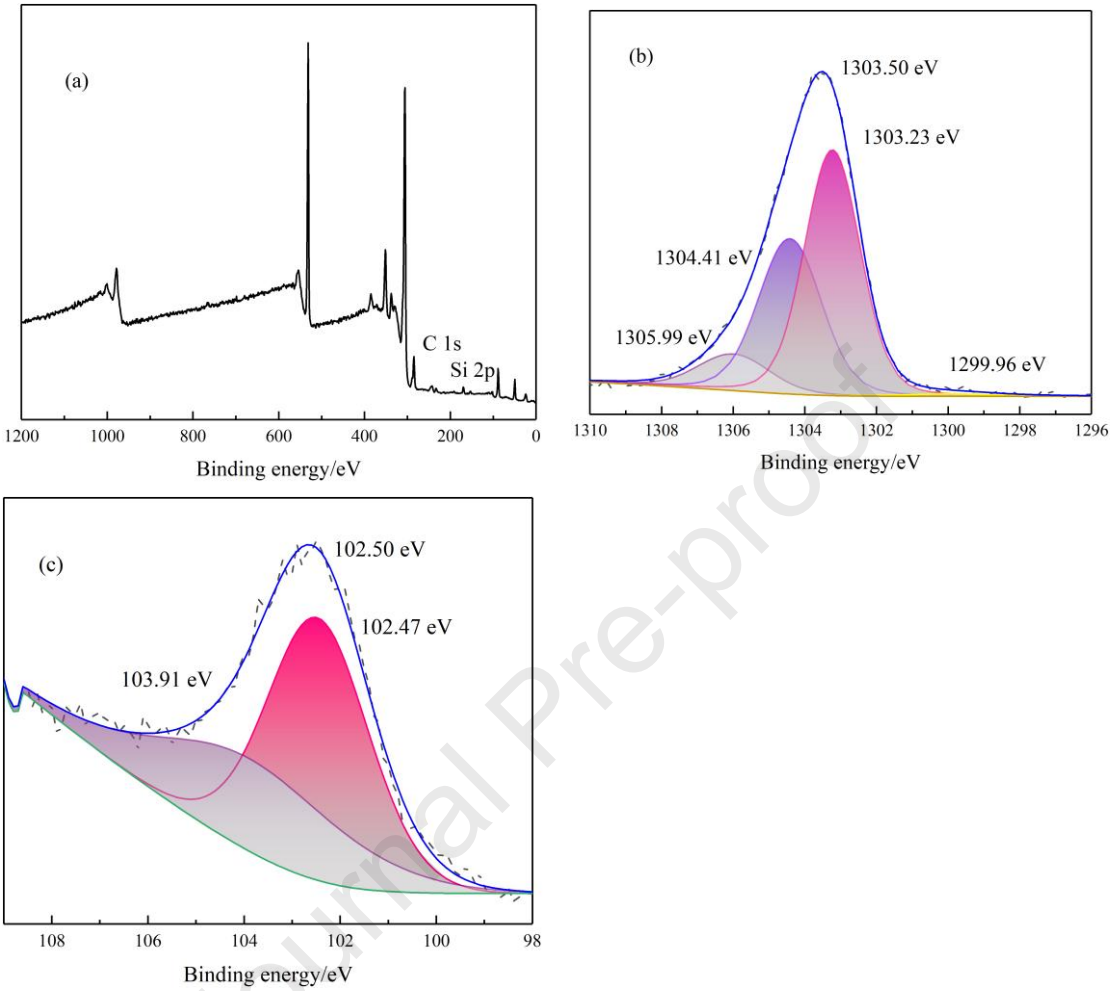

Fig. 13 XPS data of MOSFS4 after 90 d of water immersion: (a) XPS spectra; (b) Mg 1s; (c) Si 2p

Fig. 14 shows the ^{29}Si NMR spectra of MOSFS4 after 90 d of water immersion, from which the I(Q^1), I(Q^2), I(Q^3), and I(Q^4) were determined as 0.7%, 24.1%, 35.7%, and 39.5%, respectively. Compared to the I(Q^4) calculated from Fig. 6, a decrease in I(Q^4) was observed, indicating that the FS had been continuously consumed, in agreement with the findings presented in Fig. 13. The I(Q^{3a}), I(Q^{3b}), and I(Q^{3c}) were 8.8%, 7.8%, and 19.1%, respectively. The degree of polymerisation of M-S-H gel in MOSFS4 after 90 d of water immersion was calculated to be 0.45, lower than the value observed in Fig. 6, with an I(Q^3)/I(Q^2) ratio of 1.48, indicating a reduction in the proportion of M-S-H gel with the chain-like structure. The polymerisation degree of M-S-H gel decreased upon water immersion, consequently encouraging the generation of additional layered gel structures in the MOS cement. Furthermore, the ratios of I(Q^{3b}) and I(Q^{3c}) relative to I(Q^3) rose, pointing to a greater share of the talc-like (T:O:T) M-S-H gel configuration. The variation in the

Mg-Si ratio altered the distribution of I(Q^3), which consequently impacted the structural integrity of this gel's layered framework [40]. Exposure to water promoted the integration of additional MgO or $Mg(OH)_2$ into the gel-forming process, thus raising the fraction of M-S-H gel possessing a lamellar architecture.

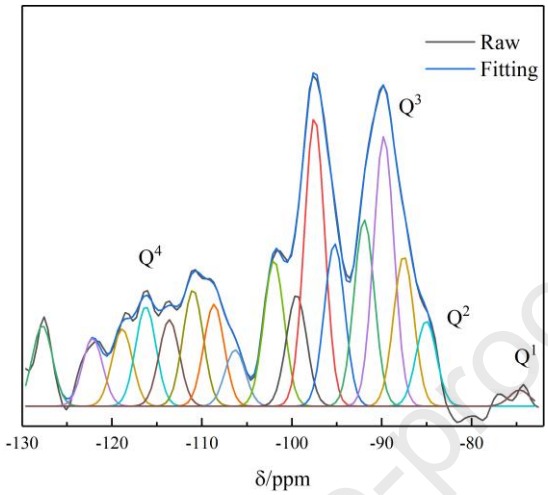

Fig. 14 ^{29}Si NMR spectra of MOSFS4

Fig. 15 presents SEM images of MOSFS4 after water immersion. Elemental mapping indicated that Si was distributed on the surface of the MOS cement matrix, with significant enrichment observed in certain areas. In addition, the detection of Si on the 5·1·7 phase implied that the evolution of incompletely formed M-S-H gel might have proceeded along this route. This observation aligned with the findings presented in Fig. 10.

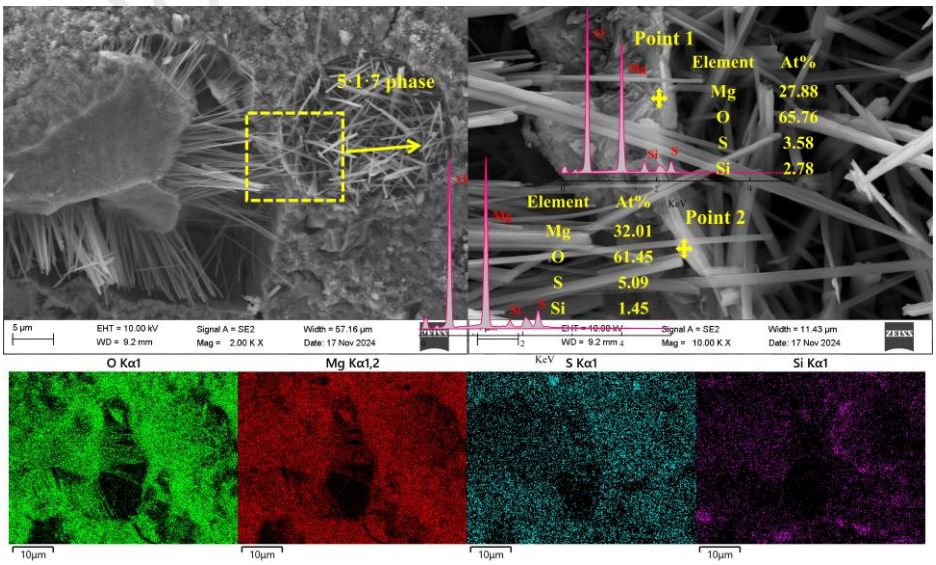

Fig. 15 SEM images of MOSFS4 after 90 d of water immersion

4 Mechanism of FS in regulating the hydration of MOS cement

FS participated in the hydration process of MOS cement and modified the evolution of the hydration products, thereby influencing the development of both mechanical properties and water resistance (Figs. 3 and 12(a)). The proposed hydration mechanism is schematically illustrated in Fig. 16. Owing to its predominantly amorphous structure and high reactivity (Fig. 1(a)), FS readily participated in the hydration process of MOS cement.

During hydration, MgO derived from LBM reacted in the presence of citric acid (CA) to produce the $5Mg(OH)_2 \cdot MgSO_4 \cdot 7H_2O$ (5·1·7) phase together with $Mg(OH)_2$ as the principal hydration products. As hydration progressed, the alkalinity of the pore solution continuously evolved. MgO hydration commenced at the particle surface, producing OH^- ions (Scheme 4 and Fig. 16), which played a crucial role in the formation of the 5·1·7 phase [19]. Under alkaline conditions, the amorphous silica in FS gradually dissolved to form $HSiO_3^-$ species, which subsequently reacted with Mg^{2+} to produce M-S-H gel [19,41]. The consumption of OH^- during FS dissolution altered the local hydration environment and partially suppressed the formation of the 5·1·7 phase (Figs. 4 and 5), whose formation depends on the self-assembly of Mg^{2+}, OH^- and SO_4^{2-} under the regulation of CA [7]. The SEM observations further support this mechanism, as M-S-H gel was detected on the surface of the 5·1·7 phase (Fig. 10(f)).

Besides MgO, $Mg(OH)_2$ may also contribute to M-S-H gel formation through its dissolution (Scheme 5) [42,43]. However, because the solubility of $Mg(OH)_2$ remains relatively low under alkaline conditions [44], its contribution is expected to be less significant than that of MgO. Previous studies have similarly shown that MgO is more effective than $Mg(OH)_2$ in promoting M-S-H gel formation [24,32,45]. Nevertheless, the variation in $Mg(OH)_2$ content observed in Fig. 5 suggests that $Mg(OH)_2$ may participate in the hydration process to a limited extent.

$$MgO + H_2O \rightarrow MgOH^+_{(surface)} + OH^- \rightarrow MgOH^+ \cdot OH^-_{(surface)} \rightarrow Mg^{2+} + 2OH^- \quad (4)$$

$$Mg(OH)_2 \rightleftharpoons Mg^{2+} + OH^- \quad (5)$$

Introducing FS into the manufacturing process of MOS cement exerted a notable influence on the formation of the 5·1·7 phase and $Mg(OH)_2$, particularly the 5·1·7 phase, which was essential for strength gain in the cementitious matrix. By influencing the hydration products, FS revealed the essential contribution of M-S-H gel to the mechanical behaviour of the hardened MOS cement matrix. As shown by the pore structure analysis (Fig. 7), increasing the FS dosage increased the proportion of pores smaller than 50 nm from 31.87% in MOSFS1 to 47.72% in

MOSFS4, indicating significant pore refinement and a denser cement matrix. Combined with the TG – DTG, XRD, and SEM results, this finding suggests that the formation of M-S-H gel effectively enhanced the compactness of the MOS cement matrix and contributed to the observed improvement in mechanical properties.

Furthermore, although the incorporation of FS partially inhibited the formation of the 5·1·7 phase, which is the principal strength-bearing hydration product in MOS cement, the formation of M-S-H gel and the accompanying matrix densification compensated for the reduction in the content and crystal size of the 5·1·7 phase. Consequently, the combined effects of pore refinement, M-S-H gel formation, and microstructural densification promoted the overall mechanical performance of MOS cement.

Dispersed Si element on the surface of the MOS cement matrix, where a notable accumulation of Si was observed (see Fig. 10(d)), suggested that the effect was not solely attributable to FS, but rather indicated a potential role of M-S-H gel formation in enhancing the matrix density (see Fig. 7). In addition, the sustained consumption of FS promoted the mechanical property enhancement of the composite (see Figs. 6 and 14). Following water immersion, the remaining MgO within the matrix transformed into $Mg(OH)_2$ (see Fig. 12(b)), which subsequently deteriorated the durability of the hardened paste. However, as FS was consumed, $Mg(OH)_2$ formation was effectively suppressed, while the $I(Q^{3a})$ of M-S-H gel was concurrently elevated. The $I(Q^3)/I(Q^2)$ of M-S-H gel varied with the Mg/Si ratio of the precursor materials, with values declining once the Mg/Si ratio rose above 0.8 [46]. During the manufacturing of MOS cement, the Mg/Si was considerably higher than 0.8. Based on the $I(Q^3)/I(Q^2)$ calculated from Figs. 6 and 14, which were 1.09, 2.14, 0.91, and 1.48 at different curing stages, the content of MgO and $Mg(OH)_2$ involved in the generation of M-S-H gel varied with curing time. Upon contact with water, a-MgO within the LBM rapidly hydrated, releasing OH^- into the system, which facilitated the dissolution of FS. The consumption of a-MgO and the establishment of solubility equilibrium for $Mg(OH)_2$ subsequently influenced the formation of M-S-H gel, leading to changes in the Mg/Si of the M-S-H gel. Pore solution pH value in MOS cement progressively stabilised with extended curing [19].

The lower $I(Q^3)/I(Q^2)$ values observed for M-S-H gel within cement at 28 d of curing could be explained by the persistent consumption of a-MgO, which did not generate enough hydroxyl

ions to accelerate FS dissolution. The results shown in Figs. 6 and 9 provided partial support, suggesting that the rate of FS consumption decreased. When Fig. 10(b) is compared with Fig. 5(b), the greater $Mg(OH)_2$ content observed in the MOSFS1 matrix points to residual MgO hydration having accelerated FS consumption, consequently boosting M-S-H gel formation and raising both the layered gel fraction and the Mg/Si value. FS, as a potential material providing the Si source, exhibited a positive effect on the water resistance of MOS cement. However, it should be noted that an excessive amount of FS does not apply to MOS cement. The strength evolution of MOS cement is sustained by both the M-S-H gel within the matrix and the 5·1·7 phase. While too much FS hindered the development of the latter, a suitable proportion effectively harmonised gel production with phase growth. Besides, FS featured low cost and stable properties, laying a solid foundation for its industrial application in high-performance MOS cement modification.

Compared with other siliceous materials, such as fly ash, silicic acid, and magnesium slag, FS contains a higher proportion of amorphous silica, resulting in greater pozzolanic reactivity [17,19,47]. Although these materials can also participate in hydration under appropriate conditions, fly ash and magnesium slag generally contain calcium-bearing phases and other impurities that may influence the hydration chemistry of MOS cement. In particular, calcium-containing phases may promote gypsum formation during water immersion, which destabilises the 5·1·7 phase, increases porosity, and consequently reduces the water resistance of MOS cement [48]. In contrast, the high-purity amorphous silica in FS provides a more direct route for promoting M-S-H gel formation while minimising undesirable side reactions.

From a practical perspective, FS is produced using a mature manufacturing process with stable quality and consistent composition, making it suitable for reproducible cement production. Although its unit cost is higher than that of industrial by-products such as fly ash or magnesium slag, it remains considerably less expensive than high-purity silicic acid. Moreover, the optimum dosage of FS identified in this study is relatively low (1–7 wt.% of LBM), which limits its contribution to the overall material cost. In addition, FS-modified MOS cement can be manufactured using conventional mixing and curing procedures without requiring additional processing equipment or specialised manufacturing conditions, further enhancing its practical feasibility.

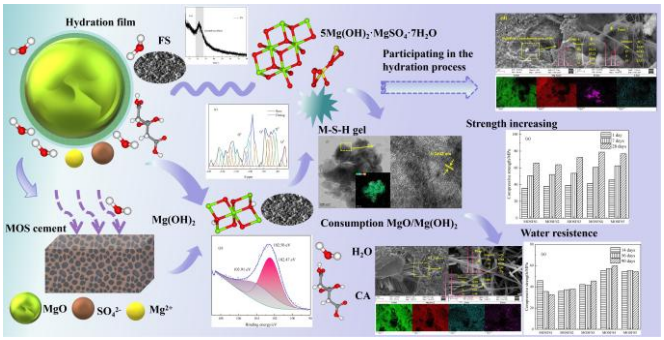

Fig. 16 Proposed hydration and strengthening mechanism of white carbon black (FS) in magnesium oxysulfate (MOS) cement

5 Conclusions

FS played the role of an active inducer, accelerating the transition of MgO/$Mg(OH)_2$ to M-S-H gel during the full curing period of the MOS cement. Unlike passive inhibition (e.g., increasing the density of MOS cement to prevent water from entering the matrix), FS actively participated in the hydration process of MOS cement, thereby aiding in the prevention of strength reduction caused by residual MgO hydration and altering the composition of the hydration products. These findings improve the understanding of the synergetic hydration of MOS with FS. Based on the experimental outcomes and the scientific investigation into the governing mechanisms, the following conclusions may be reached:

1. FS played a positive role in the progression of the engineering properties of cement. At a 5% by mass, the compressive and flexural strength of MOS cement reached 78.8 MPa and 18.9 MPa, respectively, both of which were the highest observed among all samples. After 90 d of water immersion, the compressive strength of MOS cement containing 5% FS by mass reached 57.3 MPa, exceeding that of the control specimen by 75.76%.

2. By actively engaging in the hydration reactions, FS incorporation into MOS cement densified the matrix, modified the evolution of the 5·1·7 phase and $Mg(OH)_2$, and stimulated the production of M-S-H gel. This effect can be attributed to FS's interaction with OH^- released during the MgO hydration process, which promoted its deposition on the surface of the 5·1·7 phase. This deposition resulted in a close interweaving of the 5·1·7 phase and M-S-H gel at the nanoscale, highlighting the compatibility between the 5·1·7 phase and M-S-H gel. This interplay restrained the development of the 5·1·7 phase yet provided a shielding effect that reduced its

574 dissolution to some degree. With rising FS content, the detrimental effect on the crystallite size of
575 both the 5·1·7 phase (at the (222) plane) and $Mg(OH)_2$ (at the (011) plane) grew more significant,
576 emphasising the essential contribution of M-S-H gel to the engineering property evolution of
577 MOS cement within a specific dosage range.

578 3. FS consumption remained continuous throughout curing, encompassing both air curing
579 and water immersion. During the various curing stages, the rate of FS consumption varied
580 significantly, resulting in changes in the compositions of the M-S-H gel. Consequently, the
581 proportion of M-S-H gel in different structural forms, including chain-like and layer structures,
582 also varied. Exposure to water promoted a higher content of M-S-H gel with a T:O:T layered
583 configuration in the hardened MOS cement. MgO and $Mg(OH)_2$ both participated as reactants in
584 generating this phase, which helped reduce the volumetric expansion from ongoing MgO
585 hydration and thus lessened the resulting decline in mechanical performance.

586

587 **Acknowledgement**

588 The authors would like to thank the financial support from the 2025 Science and Technology
589 Support Project of State Key Laboratory of Water Engineering Ecology and Environment in Arid
590 Area (2025GJCXPT01014), National Natural Science Foundation of China (52569024), Natural
591 Science Foundation of Inner Mongolia Autonomous Region (2026QC0604, NDYB2025-96,
592 2024MS05054), and Research on Activation and Strengthening Technology of Ecological
593 Negative Carbon Aggregates Based on Coal Mine Powder Slag (ST2024005), the UKRI under
594 grant EP/X04145X/1 (i.e., the CSTO2NE project), and the Royal Society under grant
595 IEC\NSFC\223146 to sponsor this research.

596

597 **Reference**

598 [1] Seth Pratyay, Sebastian Jose. Plants and global warming: challenges and strategies for a
599 warming world[J]. Plant Cell Reports, 2024, 43(1).

600 [2] Ostovari Hesam, Müller Leonard, Skocek Jan, Bardow André. From Unavoidable CO_2 Source
601 to CO_2 Sink? A Cement Industry Based on CO_2 Mineralization[J]. Environmental science &
602 technology,2021,55(8):5212-5223.

603 [3] Xi Jiang, Rui Xiao, Yuetan Ma, Miaomiao Zhang, Yun Bai, Baoshan Huang. Influence of

604 waste glass powder on the physico-mechanical properties and microstructures of fly ash-based
605 geopolymer paste after exposure to high temperatures[J]. Construction and Building Materials,
606 2020, 262.
607 [4] Sam A Walling, John L Provis. Magnesia-Based Cements: A Journey of 150 Years, and
608 Cements for the Future?[J]. Chemical reviews, 2016, 116(7).
609 [5] Jin Zhou, Baolan Li, Yongsheng Du, Yuanrui Li, Jinmei Dong, Chenggong Chang, Jing Wen,
610 Weixin Zheng. Review of the research progress of magnesium oxysulfate cement and its recent
611 application in green manufacturing[J]. Journal of Cleaner Production,2025,490,144751.
612 [6] Yongshan Tan, Shichang Liu, Mithila Achintha, Renjie Mi. Is It Possible to Make
613 Magnesia-Based Cement Environmentally Friendly? [J]. ACS sustainable chemistry &
614 engineering,2024,12(46):16869-16883.
615 [7] Nan Wang, Hongfa Yu, Wanli Bi, Yongshan Tan, Na Zhang, Chengyou Wu, Haiyan Ma, Shi
616 Hua. Effects of sodium citrate and citric acid on the properties of magnesium oxysulfate cement[J].
617 Construction and Building Materials,2018,169,697-704.
618 [8] Chengyou Wu, Wenhai Chen, Huifang Zhang, Hongfa Yu, Wuyu Zhang, Ningshan Jiang,
619 Lianxin Liu. The Hydration Mechanism and Performance of Modified Magnesium Oxysulfate
620 Cement by Tartaric Acid[J]. Construction and Building Materials,2017,144, 516-524.
621 [9] Xiaoyang Chen, Tingting Zhang, Christopher Cheeseman, Wanli Bi, Shaoyan Wang.
622 Production of Rapid-Hardening Magnesium Oxysulfate Cement Containing Boric Acid[J]. Journal
623 of Materials in Civil Engineering, 2022, 34(5).
624 [10] Tao Guo, Hefang Wang, Hongjian Yang, Xiaosen Cai, Qiu Ma, Shaoming Yang. The
625 mechanical properties of magnesium oxysulfate cement enhanced with 517 phase magnesium
626 oxysulfate whiskers[J]. Construction and Building Materials,2017,150,844-850.
627 [11] Nan Wang, Hongfa Yu, Wanli Bi, Yan Guan, Wei Gong, Na Zhang, Chengyou Wu. The
628 Improvement Effects of NaH_2PO_4 and KH_2PO_4 on the Properties of Magnesium Oxysulfate
629 Cement[J]. Journal of Wuhan University of Technology-Mater. Sci. Ed.,2021,36(1):50-57.
630 [12] Ling Qin, Xiaojian Gao, Wengui Li, Huan Ye. Modification of Magnesium Oxysulfate
631 Cement by Incorporating Weak Acids[J]. Journal of Materials in Civil Engineering, 2018, 30(9).
632 [13] Kang Gu, Bing Chen, Hongfa Yu, Na Zhang, Wanli Bi, Yan Guan. Characterization of
633 magnesium-calcium oxysulfate cement prepared by replacing $MgSO_4$ in magnesium oxysulfate

cement with untreated desulfurization gypsum[J]. Cement and Concrete Composites,2021,104091.

[14] Zhiming Wei, Bing Chen, Kang Gu, Zhengxian Yang. Study of untreated phosphogypsum as a fine aggregate for magnesium oxysulfate cement[J]. Construction and Building Materials, 2023, 365.

[15] Yan Guan, Zhiqi Hu, Zuhua Zhang, Jun Chang, Wanli Bi, Chris R Cheeseman, Tingting Zhang. Effect of hydromagnesite addition on the properties and water resistance of magnesium oxysulfate (MOS) cement[J]. Cement and Concrete Research,2021,143.

[16] Zhiqi Hu, Yan Guan, Jun Chang, Wanli Bi, Tingting Zhang. Effect of Carbonation on the Water Resistance of Steel Slag-Magnesium Oxysulfate (MOS) Cement Blends[J]. Materials (Basel, Switzerland),2020,13(21):5006-5006.

[17] Dezhi Wang, Kairong Jin, Nan Wang, Haiwei Zhang, Jinghui Wang, Xiangming Zhou. Compressive strength and water resistance of magnesium oxysulfate (MOS) cement incorporating magnesium slag[J]. Construction and Building Materials,2024,453,139053-139053.

[18] Qiyan Li, Linchun Zhang, Xiaojian Gao, Junyi Zhang. Effect of pulverized fuel ash, ground granulated blast-furnace slag and CO_2 curing on performance of magnesium oxysulfate cement[J]. Construction and Building Materials, 2020, 230, 116990.

[19] Tingting Zhang, Jingbin Zhang, Jun Chang, Wanli Bi, Chris Cheeseman, Xiaoyang Chen. Hydration and strength development in magnesium oxysulfate (MOS) cement incorporating silicic acid[J]. Composites Part B, 2024, 268.

[20] Kairong Jin, Chenjie Wu, Ziming Xiong, Dezhi Wang, Xiangming Zhou, Xiaoyang Chen. Impact of Cl^- on the performance of magnesium oxysulfate (MOS) cement[J]. Construction and Building Materials,2024,430,136472.

[21] Xinkuang Ning, Chengyou Wu, Hongdu Chen. Preparation and Characterization of Novel $5Mg(OH)_2{\cdot}MgSO_4{\cdot}7H_2O$ Whiskers[J]. Materials, 2022, 15(22):8018.

[22] Kang Gu, Bin Chen, Hongfa Yu, Na Zhang, Wanli Bi, Yan Guan. Characterization of magnesium-calcium oxysulfate cement prepared by replacing $MgSO_4$ in magnesium oxysulfate cement with untreated desulfurization gypsum[J]. Cement and Concrete Composites, 2021:104091.

[23] Yuan Jia, Yuxin Zou, Yaoting Jiang, Xinmei Zou, Yue Li, Yongxiang Zhou, Tingting Zhang. Effect of a Ca-rich environment on the reaction process of the MgO-activated SiO_2 system[J].

664 Cement and Concrete Composites, 2023, 136.
665 [24] Jingbin Zhang, Tingting Zhang, Chunlong Yuan, Xiaoyang Chen. Influence of MgO chemical
666 activity on the drying shrinkage of the MgO-SiO_2-H_2O system[J]. Construction and Building
667 Materials, 2024, 453, 139108.
668 [25] Kairong Jin, Xiangming Zhou, Dezhi Wang, Wanli Bi, Yu Lu, Jinghui Wang. Performance of
669 cementitious materials prepared with magnesium slag and concrete slurry waste[J]. Journal of
670 Building Engineering, 2024, 89, 109379.
671 [26] Abdullah F. Jamsheer, Kunal Kupwade-Patil, Oral Büyüköztürk, Ali Bumajdad. Analysis of
672 engineered cement paste using silica nanoparticles and metakaolin using ^{29}Si NMR, water
673 adsorption and synchrotron X-ray Diffraction[J]. Construction and Building Materials, 2018, 180,
674 698-709.
675 [27] Ellina Bernard, Hoang Nguyen. Magnesium silicate hydrate (M-S-H) stability under
676 carbonation[J]. Cement and Concrete Research, 2024, 178, 107459.
677 [28] Qiuping Li, Hongxia Ouyang, Xinghui Yang, Qi Wang, Yonghong Ding, Haichao Yu, Zhi Rao.
678 Synthesis, characterization, and photophysical properties of europium complex-functionalized
679 fumed silica and its corresponding PMMA-doped composites[J]. RSC
680 advances,2025,15(32):25885-25893.
681 [29] Ellina Bernard, Barbara Lothenbach, Christophe Chlique, Mateusz Wyrzykowski, Alexandre
682 Dauzères, Isabelle Pochard, Céline Cau-Dit-Coumes. Characterization of magnesium silicate
683 hydrate (M-S-H)[J]. Cement and Concrete Research, 2018, 116, 309-330.
684 [30] D'Espinose de la Caillerie J-B, Fripiat JJ. A reassessment of the ^{29}Si MAS-NMR spectra of
685 sepiolite and aluminated sepiolite[J]. Clay Minerals. 1994;29(3):313-318.
686 [31] Babacar Diallo, Mathieu Allix, Emmanuel Véron, Vincent Sarou-Kanian, Isabelle
687 Bardez-Giboire, Valérie Montouillout, Nadia Pellerin. Deconvolution method of ^{29}Si MAS NMR
688 spectra applied to homogeneous and phase separated lanthanum aluminosilicate glasses[J]. Journal
689 of Non-Crystalline Solids, 2018, 503.
690 [32] Yuan Jia, Baomin Wang, Zhenlin Wu, Junnan Han, Tingting Zhang, Luc J. Vandeperre, Chris
691 R. Cheeseman. Role of sodium hexametaphosphate in MgO/SiO_2 cement pastes[J]. Cement and
692 Concrete Research, 2016, 89, 63-71.
693 [34] J.F. Moulder, W.F. Stickle, P.E. Sobol, K.D. Bomben, Handbook of X-ray Photoelectron

694 Spectroscopy. A Reference Book of Standard Spectra for Identification and Interpretation of XPS
695 Data, Physical Electronics, Inc., Eden Prairie, Minnesota, 1995.
696 [35] Wenguang Zhou, Qianqian Ye, Zhezhe Zhou, Xinyan Sun, Jieyu Zhang, Jinfeng Cao,
697 Jianzhang Li. Green and efficient production of functionalized graphite reinforced magnesium
698 oxychloride cement-based materials[J]. Construction and Building Materials, 2024, 417, 135320.
699 [36] Na Zhang, Hongfa Yu, Haiyan Ma, Haoxia Ma, Mingfang Ba. The phase composition of the
700 MgO-$MgSO_4$-H_2O system and mechanisms of chemical additives[J]. Composites Part B, 2022,
701 247.
702 [37] Yuan Jia, Xinmei Zou, Yaoting Jiang, Yuxin Zou, Shuanglin Song, Jianyun Qin, Yongjing
703 Wang, Lihua Zhu. Study on the Stability of Low-Carbon Magnesium Cementitious Materials in
704 Sulfate Erosion Environments[J]. Materials, 2023, 16(11).
705 [38] Yuan Jia, Junwei Zhu, Enci Zhao, Jingxi Zhang, Shibo Li, Yaoting Jiang, Tingting Zhang,
706 Libo Liu. Study on the performance of polyester fibers modification system for low carbon
707 magnesium silicate-based cementitious materials[J]. Cement and Concrete Composites, 2025, 157,
708 10594.
709 [39] Tangwei Mi, Dhanendra Kumar,Mohamed Salman Faris, En Hua Yang. Sustainable
710 strain-hardening magnesium silicate hydrate composite[J]. Magazine of Concrete Research, 2025,
711 1-11.
712 [40] Cédric Roosz, Sylvain Grangeon, Philippe Blanc, Valérie Montouillout, Barbara Lothenbach,
713 Pierre Henocq, Eric Giffaut, Philippe Vieillard, Stéphane Gaboreau. Crystal structure of
714 magnesium silicate hydrates (M-S-H): The relation with 2:1 Mg-Si phyllosilicates[J]. Cement and
715 Concrete Research, 2015, 73, 228-237.
716 [41] D.R.M. Brew, F.P. Glasser. Synthesis and characterisation of magnesium silicate hydrate
717 gels[J]. Cement and Concrete Research, 2004, 35(1):85-98.
718 [42] Yu Zhang, Yawei Li, Yajie Dai. Formation of magnesium silicate hydrate in the
719 $Mg(OH)_2$-SiO_2 suspensions and its influence on the properties of magnesia castables[J]. Ceramics
720 International, 2018, 44(17):21365-21373.
721 [43] Sam A Walling, Hajime Kinoshita, Susan A Bernal, Nick C Collier, John L Provis. Structure
722 and properties of binder gels formed in the system $Mg(OH)_2$-SiO_2-H_2O for immobilisation of
723 Magnox sludge[J]. Dalton transactions (Cambridge, England: 2003), 2015, 44(17):8126-37.

[44] Agnieszka A. Pilarska, Łukasz Klapiszewski, Teofil Jesionowski. Recent development in the synthesis, modification and application of $Mg(OH)_2$ and MgO: A review[J]. Powder Technology, 2017, 319, 373-407.

[45] Simoni Marco, Woo Chun Long, Zhao Han, Iuga Dinu, Svora Petr, Hanein Theodore, Kinoshita Hajime, Walkley Brant. Reaction mechanisms, kinetics, and nanostructural evolution of magnesium silicate hydrate (M-S-H) gels[J]. Cement and Concrete Research, 2023, 174.

[46] Bernard Ellina, Lothenbach Barbara, Rentsch Daniel, Pochard Isabelle, Dauzères Alexandre. Formation of magnesium silicate hydrates (M-S-H)[J]. Physics and Chemistry of the Earth, 2016,99.

[47] Na Zhang, Hongfa Yu, Wei Gong, Ting Liu, Nan Wang, Yongshan Tan, Chengyou Wu. Effects of low- and high-calcium fly ash on the water resistance of magnesium oxysulfate cement[J]. Construction and Building Materials,2020,230116951-116951.

[48] Jiuye Zhao, Jiahui Xu, Chunyi Cui, Chunyang Yu, Jun Chang, Zhiqi Hu, Wanli Bi. Stability and phase transition of 5·1·7 phase in alkaline solutions[J]. Construction and Building Materials,2020,258.

- FS served as an active inducer, facilitating the transformation of MgO/$Mg(OH)_2$ into magnesium silicate hydrate gel.
- FS increased MOS cement matrix density and influenced the formation of the 5·1·7 phase and $Mg(OH)_2$, and facilitated the generation of M-S-H gel by actively participating in the hydration process.
- The structure of the magnesium silicate hydrate gel within magnesium oxysulfate cement progressively resembled that of talc (T:O:T) after water immersion.
- The mechanism of the synergetic hydration of MOS cement with FS is revealed.

Declaration of interests

☒ The authors declare that they have no known competing financial interests or personal relationships that could have appeared to influence the work reported in this paper.

☐ The authors declare the following financial interests/personal relationships which may be considered as potential competing interests: